NUMERICAL SIMULATION OF ELECTROKINETICALLY DRIVEN MICRO FLOWS

A Dissertation

by

JUNGYOON HAHM

Submitted to the Office of Graduate Studies of
Texas A&M University
in partial fulfillment of the requirements for the degree of

DOCTOR OF PHILOSOPHY

August 2005

Major Subject: Mechanical Engineering

NUMERICAL SIMULATION OF ELECTROKINETICALLY DRIVEN MICRO FLOWS

A Dissertation

by

JUNGYOON HAHM

Submitted to the Office of Graduate Studies of
Texas A&M University
in partial fulfillment of the requirements for the degree of

DOCTOR OF PHILOSOPHY

Approved by:

Chair of Committee,	Ali Beskok
Committee Members,	N. K. Anand
	Ed. Marotta
	Halit Uster
Head of Department,	Dennis O'Neal

August 2005

Major Subject: Mechanical Engineering

ABSTRACT

Numerical Simulation of
Electrokinetically Driven Micro Flows. (August 2005)
Jungyoon Hahm, B.S., Hong-Ik University;
M.S., Hong-Ik University;
M.S., University of Wisconsin-Madison
Chair of Advisory Committee: Dr. Ali Beskok

Spectral element based numerical solvers are developed to simulate electrokinetically driven flows for micro-fluidic applications. Based on these numerical solvers, basic phenomena and devices for electrokinetic applications in micro and nano flows are systematically studied. As a first application, flow and species transport control in a grooved micro-channel using local electrokinetic forces are studied. Locally applied electric fields, zeta potential patterned grooved surfaces, and geometry are manipulated to control mixed electroosmotic/pressure driven flow in the grooved micro-channel. The controlled flow pattern enables entrapment and release of prescribed amounts of scalar species in the grooves. As another application, hydrodynamic/electrokinetic focusing in a micro-channel is studied. External electric field, flow rate of pressure driven flow, and geometry in the micro-channel are manipulated to obtain the focusing point, which led to determination of the electrophoretic mobility and (relative) concentration of dilute mixtures. This technique can be used to identify and detect species in dilute mixtures.

To my Parents and my lovely Wife

ACKNOWLEDGMENTS

First of all, I would like to express my deep gratitude to Prof. Ali Beskok for his continuous encouragement, guidance, and complete academic and financial support. Thanks to him, I developed an interest in micro-fluidic and am able to apply my knowledge in this challenging field. I hope that I can always find a great boss like him.

Special thanks to my committee members, Professor N. K. Anand, Professor Ed. Marrotta, and Professor Halit Uster, for their valuable guidance and suggestions.

I would also like thank to my office mates: Paradip, Ho-jun, Ashwin, and Srinivas for their cooperation.

Finally, I am grateful to my wife, Changok Yim, for her support, love and patience. We met at Texas A&M catholic church and we cannot forget our lives in College Station.

I would like to express my appreciation for the *continous* love and support of my parents, Dr. Young-il Hahm and Mrs. Hea-sook Um, from Korea. They always encourage and inspire me.

TABLE OF CONTENTS

CHAPTER Page

LIST OF TABLES

LIST OF FIGURES

FIGURE Page

FIGURE Page

CHAPTER I

INTRODUCTION

A. Background

Micro-fluidics is an emerging technology that allows development of new approaches to synthesize, purify, and rapidly screen chemicals, biologicals, and materials using integrated, massively parallel, miniaturized platforms. These properties allow micro-fluidics to be used in nanotechnology applications in a top-to-down approach, where micro-scale processes are utilized for fabrication, assembly and manipulation of nano-scale components. Particularly, "micro total analysis systems" (μTAS) developed for drug delivery, DNA analysis and sequencing, and biological/chemical-agent detection are most suitable for nanotechnology use. Most μTAS utilize a combination of electrokinetic transport mechanisms for particle and species manipulation and bulk flow control. Electrokinetic micro flows are often encountered in micro-fluidic applications. The electrokinetic phenomena can be divided into the following four categories [1]:

- Electroosmosis is the motion of ionized liquid relative to the stationary charged surface by an applied electric field.
- Electrophoresis is the motion of the charged surfaces and macromolecules relative to the stationary liquid by an applied electric field.
- Streaming potential is the electric field created by the motion of ionized fluid along stationary charged surfaces (opposite of electroosmosis).
- Sedimentation potential is the electric field created by the motion of charged

---

The journal model is *IEEE Transactions on Automatic Control.*

Table I. Typical physical and electrochemical parameters utilized in electrokinetically driven phenomena.

Parameter	Parameter range
Typical channel half height, h (μm)	$0.1 \sim 100$
Electrolyte concentration, n_o (mM)	$100 \sim 0.01$
Debye length, λ (nm)	$1 \sim 100$
Zeta potential, ζ (mV)	$\pm 25 \sim \pm 100$
Electric field, $\vec{E}$ (V/mm)	$1 \sim 100$
Reynolds number, Re	$10^{-4} \sim 1$

particles relative to a stationary liquid (opposite of electrophoresis).

Among them, electroosmosis and electrophoresis are the two mostly utilized electrokinetic effects in micro- and nano-scale transport applications [1, 53] with typical physical and electrochemical conditions given in table I.

B. Electroosmosis

Electroosmosis is the process of inducing motion of ionized liquid relative to a stationary charged surface using an applied electric field. It is the leading electrokinetic phenomenon utilized in micro-fluidic systems. It enables fluid handling and flow control through selective applications of electric fields in micro-channel systems, eliminating moving mechanical components and significantly reducing mechanical failure modes due to fatigue and fabrication defects. Electroosmotic pumping is commonly utilized in microchip-based sensors for detection of biological/chemical agents, and for various biomedical pumping and drug delivery applications.

1. Review of Recent Developments for Electroosmosis

In this section, we present an extended literature survey on electroosmotic transport, covering the theoretical, experimental and numerical modeling aspects of electroosmosis. This is followed with discussions on various issues, such as electroosmosis suppression with Zeta potential modifications, and recent efforts on development of micro-mixers using electroosmotic effects.

Liquid flows in capillary porous systems under the influence of external electric fields have attracted the attention of many scientists, since the discovery of electrokinetic transport by Reuss in 1809 [2]. In 1870, Helmholtz developed the electric double layer theory, which relates the electrical and flow parameters for electrokinetic transport. Electroosmosis has been used for chemistry applications since the late 1930's.

Theoretical developments include solution of mixed electroosmotic/pressure driven flows in very thin two-dimensional slits [3, 4, 5], as well as in thin cylindrical capillaries [6, 7, 8]. In 1952, Overbeek proposed irrotationality of internal electroosmotic flows for arbitrarily shaped geometries [9]. This is followed by the ideal electroosmosis concept (i.e., electroosmotic flow in the absence of externally imposed pressure forces) by Cummings et. al. [10], who have shown the similarity between the electric and velocity fields under *specific* outer field boundary conditions. More recently, Santiago has shown that ideal electroosmosis is observed for low Reynolds number, steady flows. However, unsteady or high Reynolds number flows violate this condition [11]. Analytical solution of unsteady electroosmotic flows obtained by Dutta and Beskok confirms predictions of Santiago [12].

Time periodic electroosmotic flows, also known as AC electroosmosis, is driven by an alternating electric field. Literature on time periodic electroosmotic flows have

been quite limited. Dose and Guiochon reported numerical results for impulsively started electroosmotic flow [13]. Soderman and Jonsson presented analytical results for starting electroosmotic flows in a semi-infinite domain, two-dimensional channels and pipes [14]. Green et. al. investigated AC electroosmosis on planner micro-electrodes using steady and unsteady electric fields [15]. In a later study, they analyzed the same problem based on the linearized Debye layer theory [16]. Barragan and Bauza reported experimental results of sinusoidally alternating electroosmotic flows, super-imposed onto a steady electroosmotic flow [17]. Dutta and Beskok obtained analytical solutions of AC electroosmosis in two-dimensional straight channels, valid for a wide range of actuation frequencies [12]. They have identified similarities between the AC electroosmotic flows and bounded Stokes layers in the bulk flow region.

A brief review of the recent experimental work is as follows: Molho et. al. presented measurements of electroosmotically driven micro-capillary flows, and they have shown that Joule heating and the corresponding changes in fluid viscosity are secondary effects compared to the streamwise pressure gradients [18]. The same year, Paul et. al. have used caged dye fluorescence technique to capture the flow patterns in mixed electroosmotic/pressure driven micro-channel flows [19]. Cummings and co-workers have used micro-particle image velocimetry (μPIV) technique to obtain velocity distribution in straight channels and cross flow junctions [20]. Kim et. al. have also developed a μPIV technique, and utilized this to measure mixed electroosmotic/pressure driven flows in cross-flow and T-junctions [21]. Most recently, Singh et. al. developed unilamellar liposome particles to trace micro-flows [22]. Unlike the traditional latex flow marker. These contain fluorescent material both in the core and at the surface of the marker. Hence this technique provides higher fluorescence intensity.

Herr et. al. reported velocity and dispersion rate measurements for electroos-

motic flows through cylindrical capillaries with non-uniform surface charge distribution [23]. They have used various surface materials as well as polymeric coatings to obtain different surface charge distribution by modifying the local Zeta potential. Experiments performed using caged-dye fluorescence technique, indicated strong dependence of fluid velocity and dispersion rate on the surface charge distribution [23]. In electrokinetic flows, fluid dispersion may also be caused by a mismatch in the electroosmotic flow rate and electric field. It can also be induced by Joule heating.

There has been numerous studies on numerical simulation of electroosmotic transport. Yang and Li developed a numerical algorithm based on the Debye-Hückel linearization, and studied electrokinetic effects in pressure driven liquid flows [24]. Numerical simulations of micro-fluidic injection using electroosmotic forces through intersection of two channels were presented by Patankar and Hu, using a finite volume algorithm [25]. Their numerical results for $Re > 1$ flows showed significant inertial effects, which is in agreement with the theoretical work of Santiago [11]. Bianchi et. al. used finite element formulation to model electroosmotic flow in a T-channel junction [26]. Beskok and colleagues have developed a spectral element algorithm for solution of mixed electroosmotic/pressure driven flows in complex geometries [27, 28].

Although electroomosis is an attractive technique for micro-fluidic pumping, it may need to be suppressed or modified for certain applications, such as the capillary isoelectric focusing (IEF) and on-chip IEF, by altering the Zeta potential. This can be obtained by various techniques, including polymer coatings and embedded surface electrodes. The details of this will be discusseed in section A of Chapter IV.

C. Electrophoresis

Electrophoresis is the process of inducing motion of charged particles relative to a stationary liquid using an applied electric field, where the liquid acts as a conducting medium. The velocity at which charged particles/molecules move towards the anode or cathode is known as the electrophoretic migration velocity. This motion is determined by a balance between the driving Coulomb forces due to the net particle charge, and the opposing viscous drag. Therefore, electrophoretic migration velocity is proportional to the applied electric field and the net charge of the molecule, and it is inversely proportional to the viscosity of the liquid and the size of the particle. Electrophoresis is commonly used in species separation and separation based detection of biological and chemical entities, especially DNA and protein macromolecules [42, 43, 44]. In this section, we will review the recent experimental and numerical modeling efforts of electrophoretic transport.

1. Review of Recent Developments for Electrophoresis

Electrophoresis is one of the most extensively used electrokinetic phenomena for separation and/or characterization of charged particles, as well as biological molecules. For example, proteins, amino acids, peptides, necleotides and polynucleotides can be separated using electrophoretic techniques. The electrophoresis can be divided into three major categories. These are the moving boundary, steady state, and zone electrophoresis [45].

Moving boundary electrophoresis is a widely used technique in commercial and laboratory setups, where the solution containing positively and negatively charged particles are subjected to electric fields, and the particles move towards the oppositely charged electrode. This results in motion of the solution boundary, which is commonly

detected using Schleiren optical techniques. Steady state electrophoresis is obtained, when the positions of separated components do not change in time [45]. Steady state electrophoresis is commonly observed in isoelectric focusing (IEF) applications. In IEF, charged particles migrate under electrophoretic forcing and pH gradients to a location in the buffer, where they experience zero net charge. This location is known as the isoelectric point [46, 47, 48, 49]. Zone electrophoresis utilize a supporting medium to hold the sample, while an external electric potential is applied at the end of the supporting media. Typically, filter paper, cellulose, cellulose-acetate and gel are used as the supporting media [50].

Electrophoresis is commonly applied in capillaries and micro-scale channels [51]. Advantages of capillary electrophoresis was highlighted in the early 1980's by the work of Jorgenson and Lukacs, where electrophoretic separations in capillaries were shown to offer the potential for development of automated analytical equipment with fast-analysis time and on-line detection possibilities. Today, many separation techniques rely on combined capillary electrophoresis and electroosmotic flow to pump solutes towards the detector. Through a set of experiments, Polson and Hayes demonstrated flow control using external electric fields in capillary electrophoresis [52]. They prescribed a certain orientation of electrodes, which significantly reduced the external electric field, and hence, increased the electrophoretic separation efficiency. Ramsey and co-workers have developed a micro-fluidic array for E.coli detection. This device utilized pure electrophoretic transport [33].

This thesis is organized as follows. In Chapter II, we review the governing equations for electrokinetics including flow and species transport. In Chapter III, we present nondimensionalization and discretization of the governing equations using spectral element method (SEM). In Chapter IV, we demonstrate flow and species transport central in grooved micro-channels using local electrokinetic effect. In Chap-

ter V, we present a new microfluidic device concept for electrophoretic mobility and (relative) concentration measurements of dilute mixtures. Finally, conclusion of our research and future work are presented.

D. Nomenclature

c Concentration of scalar species

c_i Concentration of i^{th} species

c^* Nondimensional concentrationof species transport

D Dielectric constant

D_i Diffusion coefficient of i^{th} type ion

$\vec{E}$ Electric field

e Electron charge

F Faraday's constant

f_{ek} Electrokinetic body force

h Half channel height

k Thermal conductivity

k_b Boltzmann constant

L Length of splitter in mobility device

ΔL Increment of length for inner splitter in mobility device

n_i Ion density of i^{th} type

n_o Average number of ions per unit volume

P Pressure

p^* Nondimensional pressure

Pe Peclet number, $ReSc$

Pr Prandlt number

Sc Schmidt number

$\dot{q}$ Volumetric flow rate per channel width W

Re Reynolds number

T Absolute temperature

t Time

u^* Nondimensional streamwise velocity,u/u_p

U_0 Nondimensional inlet velocity

u Stream wise velocity component

u_0 Streamwise velocity at the inlet

u_{HS} Helmholtz Smoluchowski velocity

$\bar{u}$ Averaged channel velocity

$v^*($ Nondimensional cross stream velocity

$\vec{u}$ Velocity vector

v Cross stream velocity component

v_j ion velocity

v_{tj} Total velocity of j^{th} type ion

y Distance measured from the wall

z Valance

Greek Letters

α Ionic energy parameter, $\frac{ez\zeta}{k_bT}$

β Non dimensional parameter relating α, ω, and h

α_q Integration weight for numerical formulation

β_q Integration weight for numerical formulation

ϵ Permittivity

ϵ_0 Permittivity of vacuum

ϕ External electric potential

η Nondimensional cross flow distance, y/h

λ Debye length, $1/\omega$

μ Dynamic viscosity

μ_{ek} Electrokinetic mobility

μ_{eo} Electroosmotic mobility

μ_{ep} Electrophoretic mobility

ν Kinematic viscosity

t^* Nondimensional time

ρ_q Electric charge density

ρ_f Fluid density

σ Electric conductivity

ω Debye Hückel parameter

ξ Non-dimensional stream wise distance, x/h

ψ Electroosmotic potential

ψ^* Non-dimensional electroosmotic potential, ψ/ζ

ψ_o Surface charge potential

ζ Zeta potential

CHAPTER II

GOVERNING EQUATIONS FOR ELECTROKINETICS

A. Governing Equations

In this chapter, we review the governing equations for flow and species transport under electrokinetic effects. We first present the electric double layer, which plays a significant role in electrokinetic transport and we can obtain the corresponding electoomotic potential. Then we present a simplified treatment of the external electric field, followed with conservation laws for fluid and species transport and we can obtain external electric potential. We will utilize these governing equations in the upcoming sections, to obtain numerical models for electroosmosis and electrophoresis in micro-flows.

1. Electric Double Layer

Electrokinetic phenomena are present due to the *electric double layer* (EDL), which forms as a result of the interaction of ionized solution with static charges on dielectric surfaces [5]. For example, when silica is in contact with an aqueous solution, its surface hydrolyzes to form silanol surface groups. These groups may be positively charged as $Si-OH_2^+$, neutral as $Si-OH$, or negatively charged as $Si-O^-$, depending on the pH value of the electrolyte solution. If the channel surface is negatively charged (such as in the case of deionized water), the positive ions are attracted towards the surface, and the negative ions are repelled from the surface, keeping the bulk of the liquid, far away from the wall, *electrically neutral*. The distance from the wall, where the electrokinetic potential energy is equal to the thermal energy is known as the Debye length (λ). The Debye length depends on the molar concentration of the ionized fluid,

and its thickness λ can be estimated using the Debye-Hückel parameter (ω):

$$\omega = \frac{1}{\lambda} = \sqrt{\frac{e^2 \Sigma_i c_i z_i^2}{\epsilon \epsilon_o k_b T}}. \tag{2.1}$$

where c is the concentration, k_b is the Boltzmann constant, e is the electron charge, z is the valence, T is the temperature, ϵ_o is the dielectric permittivity of vacuum, and ϵ is the dielectric constant of the solvent. The subscript i indicates the i^{th} species. Using equation (3.5) and assuming symmetric electrolyte at $c_o = 1.0 \times 10^{-2}, 1.0 \times 10^{-5}$ and $1.0 \times 10^{-6} M$, we obtain Debye lengths of $\lambda = 3nm, 100nm$ and $300nm$, respectively [53, 47]. The EDL consists of two distinct zones: Stern- and diffuse-layers. The Stern-layer is formed due to strong attraction of ions onto the oppositely charged surface. The ions are immobilized near the charged surfaces, and the electrokinetic potential drops rapidly across the Stern-layer to a value at the edge of the Stern-layer, known as the Zeta potential (ζ). Ion redistribution in the diffuse layer results in net electric charge, which can be characterized by the electrokinetic potential ψ, and this equation is known as Poisson-Boltzmann equation ([1])

$$\nabla^2 \psi = \frac{-\rho_q}{\epsilon \epsilon_o}. \tag{2.2}$$

The electric charge density ρ_q, is given by

$$\rho_q = F \sum z_i c_i, \tag{2.3}$$

where F is the Faraday's constant. Ionic charge density can be obtained from the Nernst-Planck ion conservation equation, and is presented as:

$$\rho_q = -2 n_o e z sinh(\frac{e z \psi}{k_b T}), \tag{2.4}$$

where n_o is the ion concentration in the bulk solution for both positively and negatively charged ions, e is electron charge. Here we emphasize that net electric charge contained in the diffuse layer is the primary reason for electrokinetic effects, where charged ions or particles can be mobilized by externally applied electric fields.

In section B, we will present a model for the electric charge distribution by assuming equilibrium (Boltzmann) distribution for a symmetric electrolyte. Under these conditions, equation 2.2 will be identified as the Poisson-Boltzmann equation, and the Zeta potential will be used as the boundary condition at the edge of the Stern layer. A schematic view of the EDL structure and the corresponding electrokinetic potential distribution are shown in figure 1. The Zeta potential and ion concentration are the two most important parameters in electrokinetic transport. Electroosmotic (electroosmotic velocity per electric field strength) is proportional to the Zeta potential. Ion concentration is used in determination of the EDL thickness, which is an intrinsic length scale for electrokinetic transport. The effects of charge distribution described by the electrokinetic potential is felt deeper than the Debye length (λ), estimated by equation (3.5). Dutta and Beskok, have shown that the electrokinetic potential drops to 1% of its original (Zeta potential) value within an effective EDL thickness of about 4.5λ [5].

For micro-fluidic applications, the EDL thickness is considerably smaller than the typical micro-channel dimensions. However, presence of the EDL significantly affects performance of the micro-fluidic devices. Due to the disparity in length scales between the EDL and the typical channel size (See table 1), the EDL effects are usually incorporated in the boundary conditions. However, there are recent efforts to measure electrokinetic flows in nano-scale channels, where the channel dimensions are comparable to the EDL thickness. Hence the diffuse layers, present at channel walls, start to interact with one another. Preliminary experimental data for these

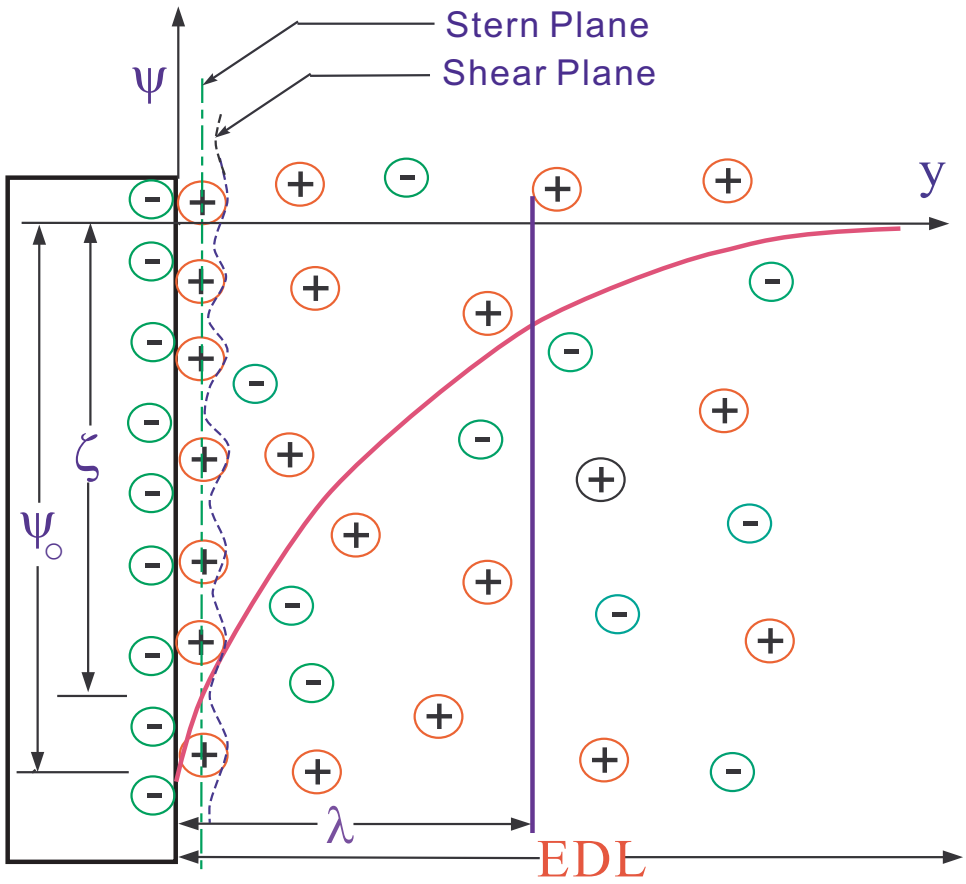

Fig. 1. Schematic diagram of the electric double layer (EDL) next to a negatively charged solid surface. Here ψ is the electrokinetic potential, ψ_o is the surface electric potential, ζ is the Zeta potential, and y is the distance measured from the wall. The Debye length and the EDL thickness are shown by λ and EDL, respectively.

cases show deviations from the classical Poisson-Boltzmann equation [54].

2. External Electric Field

In electrokinetic transport, the total electric field can be divided into two components: One due to the externally applied electric field, and the other due to the presence of the electric double layer. We already covered the latter in section 1. Hence we will concentrate on the externally applied electric field ($\vec{E}$) in this section. For simplicity, we assume that $\vec{E}$ is determined by the laws of electrostatics. Using Gauss law, we obtain

$$\nabla \cdot \vec{E} = 0. \tag{2.5}$$

The right hand side of the equation is zero, since the electric charge density (ρ_q) contained in the EDL is already included in equation (2.2). Assuming no magnetic fields and using Faraday's law, the electric field can be represented as

$$\vec{E} = -\nabla\phi, \tag{2.6}$$

where ϕ is the externally applied electric potential. These two equations are combined to result in

$$\nabla^2\phi = 0. \tag{2.7}$$

Solutions of this equation require specification of the electric potential on electrode surfaces, and no-penetration conditions on the dielectric surfaces ($\frac{\partial\phi}{\partial n} = 0$).

For most general purposes, the electric conductivity depends on the concentration of the species. Therefore, local concentration variations affect the electric conductivity, which may become important within the EDL region due to the increased ion concentration.A similar phenomenon may exist in electrophoretic transport, if

the sample concentration is comparable to the buffer concentration. Despite these limitations, most micro fluidic models assume constant electric conductivity

Recent applications of electrokinetic micro-flows utilize unsteady electric fields. Also, there has been several applications based on combined electric and magnetic fields. For such cases, the current treatment of the electric field may not be appropriate. Hence, one must utilize Maxwell's equations, instead. However, results of the current section may be useful for sufficiently low frequencies, where quasi-steady electric fields are used to generate unsteady or time-periodic flow and transport processes. This practice is acceptable due to the significant differences between the mass/momentum transport and electrostatic time-scales.

3. Conservation Laws

Assuming incompressible Newtonian fluid with constant viscosity, the bulk fluid motion is governed by the incompressible Navier-Stokes equations [1]

$$\rho_f(\frac{\partial \vec{u}}{\partial t} + (\vec{u}\cdot\nabla)\vec{u}) = -\nabla p + \mu\nabla^2\vec{u} + f_{ek}, \tag{2.8}$$

where p is the pressure, and $\vec{u}$ is a divergence free velocity field ($\nabla\cdot\vec{u}=0$) subject to the no-slip boundary conditions on the walls, ρ_f is the fluid density, and f_{EK} is the electrokinetic body force. A general equation for the electrokinetic force per unit volume is given by[55]

$$f_{ek} = \rho_q\vec{E} - \frac{1}{2}\vec{E}^2\epsilon_o\nabla\epsilon + \frac{\epsilon_o}{2}\nabla(\rho_f\frac{\partial\epsilon}{\partial\rho_f}\vec{E}^2), \tag{2.9}$$

where $\vec{E}$ is the externally applied electric field. The last term shows permittivity variations with density, and it is especially important at liquid/gas interface, as well as in ionized gas flows [55]. For our purposes, we will assume incompressible medium with constant electric permittivity. Hence we only consider contribution of the first

term ($\rho_q \vec{E}$).

Species conservation equation for multi-component fluid, in absence of chemical reactions can be expressed as:

$$\frac{\partial c_i}{\partial t} + \nabla \vec{j}_i = 0, \tag{2.10}$$

where c_i is the concentration of the i^{th} species and $\vec{j}_i$ is the species flux given by

$$\vec{j}_i = -D_i \nabla c_i + c_i[\vec{u} + \mu_{ek,i}\vec{E}], \tag{2.11}$$

where D_i is the diffusion coefficient, while μ_{ek} is the electrokinetic mobilities. First term on the right hand side shows molecular diffusion flux due to the concentration gradient, while the second term shows convection due to bulk fluid motion with velocity $\vec{u}$. The following terms represent transport due to electrokinetic and dielectrophoretic effects. In general, the electrokinetic mobility (μ_{ek}) includes both the electroosmotic and electrophoretic effects (See [56] for details). Mobility is related to the electrokinetic migration velocity $\vec{u}_{ek}$ by

$$\vec{u}_{ek} = \mu_{ek}\vec{E} \tag{2.12}$$

and it depends on physical and chemical properties of the particle/surface and the suspending fluid.

The electroosmotic mobility for infinitesimally thin EDL is given by the Helmholtz-Smoluchowski relation [53]:

$$\mu_{eo} = \frac{-\zeta\epsilon}{\mu}, \tag{2.13}$$

where ζ is the Zeta potential. Using electroosmotic mobility, we obtain the the

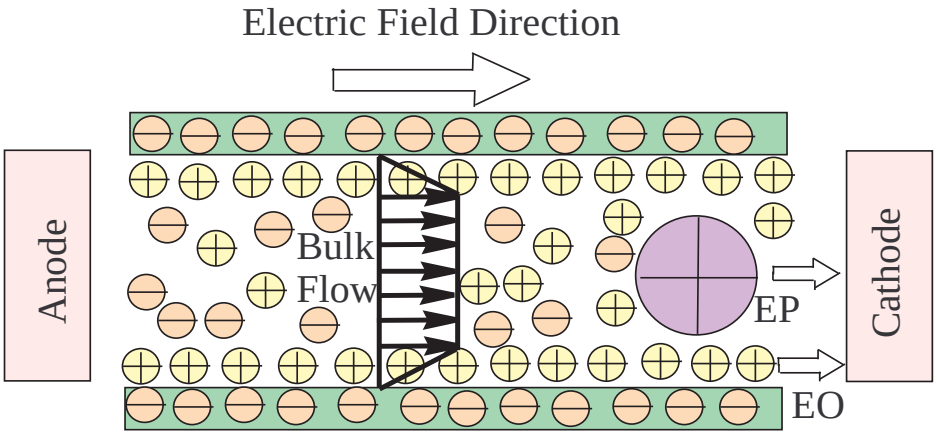

Fig. 2. A schematic view of electroosmotic and electrophoretic transport processes.

Helmholtz-Smoluchowski electroosmotic velocity (sometimes also indicated as U_{HS})

$$\vec{u}_{eo} = \mu_{eo}\vec{E} = \frac{-\zeta\epsilon}{\mu}\vec{E}. \tag{2.14}$$

Negative sign is due to the use of surface Zeta potential. For example, for a negatively charged surface ($\zeta < 0$), the EDL will be positively charged, and the resulting electroosmotic motion will be towards the cathode, as schematically shown in figure 2.

The electrophoretic mobility due to Hückel is [53]:

$$\mu_{ep} = \frac{2\zeta\epsilon}{3\mu}, \tag{2.15}$$

where the 2/3 coefficient is appropriate for particles (Note that electrophoretic mobility for macro-molecules is mostly determined experimentally). This results in electrophoretic migration velocity of

$$\vec{u}_{ep} = \mu_{ep}\vec{E}. \tag{2.16}$$

Based on this, a positively charged particle ($\zeta > 0$) that is free to move, will migrate towards the cathode, as schematically shown in figure 2.

4. Governing Equations for Electroosmotic Flow

The governing equations for electroosmosis are based on the following assumptions and approximations:

- The fluid viscosity is *independent of the shear rate*. Hence, Newtonian fluid is assumed.
- The fluid viscosity is *independent of the local electric field strength*. This condition is an *approximation*. Since the ion concentration and the electric field strength within the EDL is increased, the viscosity of the fluid may be affected. However, such effects are neglected in the current analysis, which considers only the dilute solutions.
- Ions are in equilibrium with the electric charge on the wall. Hence the Poisson-Boltzmann equation is utilized for electrokinetic potential distribution.
- The solvent is continuous and its permittivity is not affected by the overall and local electric field strength.
- The ions are point charges.
- Constant electric conductivity is assumed.
- Joule heating is neglected.

Based on these assumptions, the electroosmotic flow is generated when an external electric field ($\vec{E} = -\nabla\phi$) is applied in the presence of the EDL. This external electric field interacts with the electric double layer, and creates the electrokinetic

body force on the bulk fluid. The motion of ionized, incompressible fluid with electroosmotic body forces are governed by the incompressible Navier-Stokes equations:

$$\rho_f(\frac{\partial \vec{u}}{\partial t} + (\vec{u}.\nabla)\vec{u}) = -\nabla p + \mu\nabla^2\vec{u} + \rho_q\vec{E}, \tag{2.17}$$

where p is the pressure, and $\vec{u} = (u, v)$ is a divergence free velocity field ($\nabla \cdot \vec{u} = 0$) subject to no-slip boundary conditions on the walls, and ρ_f is the fluid density. Here ρ_q is determined from (2.4). The externally imposed electric potential (ϕ) is governed by

$$\nabla \cdot (\sigma\nabla\phi) = 0, \tag{2.18}$$

where σ is the conductivity, and the electric potential is subject to the insulating boundary conditions ($\nabla\phi \cdot \vec{n} = 0$) on the dielectric surfaces.

5. Governing Equations for Electrophoretic Transport

The governing equations for electrophoretic transport are based on the following assumptions and approximations:

- Sample concentration is small compared to the buffer concentration, and the buffer concentration and buffer pH value are uniform.
- Conductivity of the solution (σ) is uniform throughout the liquid volume.
- Concentration of the buffer solution is large enough so that the EDL thickness on channel walls is negligible, compared to the channel dimensions.
- The temperature of the solution is uniform, and Joule heating is insignificant (For details on Joule heating see [58], where an empirical formula for temperature rise due to Joule heating, as a function of the electric field, electric

conductivity, buffer and wall thermal conductivity given).

- Thermophysical parameters, such as the diffusion coefficients, fluid viscosity, electrokinetic mobilities, and dielectric properties are constant.

Using these assumptions and approximations, the species transport equation is reduced to [59, 56]:

$$\frac{\partial c_i}{\partial t} + \nabla(c_i\vec{u} + c_i\vec{u}_{ep,i}) = D_i\nabla^2 c_i, \tag{2.19}$$

where $\vec{u}_{ep,i} = \mu_{ep,i}\vec{E}$ is the electrophoretic migration velocity. Our model includes the electrophretic transport effect by adding electrophoretic velocity term in the species transport equation. To obtain velocity and species field we first determine the electric field ($\vec{E}$)using equation (2.7), and the hydrodynamic velocity $\vec{u}$, is found by solution of the incompressible Navier-Stokes equations (2.8). We obtain the species concentration from the species transport equation (2.19).

CHAPTER III

NUMERICAL FORMULATION

In this chapter, we present numerical formulation for the governing equations of previous chapter is shown. Numerical solution of electrokinetically driven flows is challenging due to the disparities between the EDL and flow length scales ($\lambda << h$), and the exponential non-linearity of the Poisson-Boltzmann equation (3.2). Small EDL thickness compared to the typical flow domain size requires accurate numerical resolution of large velocity gradients near the surfaces. This also relates to accurate solution of the Poisson-Boltzmann equation, which predicts the electric charge density (ρ_e) term used in the Navier-Stokes equations (2.8). We addressed these numerical challenges by developing an algorithm based on the spectral element method (SEM). In the SEM, we discretize the computational domain into quadrilateral elements, similar to the (low-order) finite element method (FEM). However, we further discretize each element using interpolation polynomials based on a specific set of Jacobi polynomials. This choice enables variation of the order of expansion within each element. Increasing the order of each element without changing the number of elements is known as the p-type refinement. Increasing the number of elements while keeping elemental expansion order the same, is known as the h-type refinement. Although both refinement techniques result in increased accuracy, p-type refinement leads to *exponential reduction* of discretization errors (spectral convergence), while h-type refinement results in algebraic convergence [68]. Spectral convergence is an important advantage of the SEM, since it is possible to reduce the discretization errors by at least two orders of magnitudes by simply doubling the degrees of freedom per element. Our flow solver utilizes the operator splitting scheme, and results in third-order time and spectral spatial-accuracy [67]. Further details of our numerical formulation, and code

verification can be found in [66, 28, 73]. Code validation based on comparisons with experimental data was presented in [21]. All results presented in the next chapters were tested for grid independence by successive p-type refinements.

A. Nondimensionalization

For parametric studies, we introduce the non-dimensional parameters:

$$x^* = \frac{x}{h},\ y^* = \frac{y}{h},\ t^* = \frac{t}{h/u_{HS}},\ u^* = \frac{u}{u_{HS}},\ p^* = \frac{p}{\rho_f u_{HS}^2},\ \phi^* = \frac{\phi}{\zeta},\ \psi^* = \frac{\psi}{\zeta}, \tag{3.1}$$

In here, the length scales (x, y) are non-dimensionalized using the half channel height (h), and the time scale (t^*) is non-dimensionalized using convective time. Both electric potential due to the external electric field (ϕ^*) and electric potential from the surface charge (ψ^*) are non-dimensionalized with the Zeta potential (ζ).

Based on this, the non-dimensional governing equation for electric potential becomes

$$\nabla^2(\psi^*) = \frac{-4\pi h^2 \rho_e}{D\zeta} = \beta sinh(\alpha\psi^*), \tag{3.2}$$

where α is ionic energy parameter and it is defined as:

$$\alpha = \frac{ez\zeta}{k_b T}, \tag{3.3}$$

The spatial gradients are non-dimensionalized with a characteristic length h and the parameter β relates the ionic energy parameter α,

$$\beta = \frac{1}{\alpha}(\frac{h}{\lambda})^2, \tag{3.4}$$

where the Debye length can be predicted using the

$$\frac{1}{\lambda} = \sqrt{\frac{8\pi n_o e^2 z^2}{D k_b T}}, \tag{3.5}$$

In equation (3.1), the velocity(u) is normalized using the Helomholtz-Smoluchowski velocity

$$u_{HS} = -\frac{\epsilon \zeta E_x}{\mu}, \tag{3.6}$$

where ϵ is the permittivity of the electrolyte. The pressure is normalized using the dynamic head ($\rho_f u_{HS}^2$).

Assuming incompressible Newtonian fluid with constant viscosity, the electroosmotic flow satisfies the continuity and the Navier-Stokes equations:

$$\nabla \cdot \vec{u^*} = 0, \tag{3.7}$$

$$(\frac{\partial \vec{u^*}}{\partial t^*} + (\vec{u^*}.\nabla)\vec{u^*}) = -\nabla p^* + \frac{1}{Re}\nabla^2 \vec{u^*} + \vec{F}_{EO}, \tag{3.8}$$

where p^* is the pressure, and $\vec{u^*}$ is the velocity field subjected to the no-slip boundary conditions on the walls, $Re = \frac{\rho_f u_{HS} h}{\mu}$ is the Reynolds number, ρ_f is the fluid density, and $\vec{F}_{EO}$ is the electroosmotic body force.

We now consider the species transport equation:

$$\frac{\partial c_i^*}{\partial t^*} + (\vec{u^*}) \cdot \nabla c^* = \frac{1}{Pe}\nabla^2 \quad c_i^* \tag{3.9}$$

$$\tag{3.10}$$

where $\vec{u^*}$ is the fluid velocity, and $Pe = \frac{h \cdot u_{HS}}{D}$ is the Peclet number. The i^{th} concen-

tration is nondimensionalized as

$$c_i^* = \frac{c_i}{c_0},$$

where c_o is a reference concentration level.

B. Temporal Discretization

The operator splitting scheme used in our code is an extension of a third-order stiffly stable time integration scheme developed by Karniadakis et.al, [67]. Here, we also consider the species transport equation, which includes the electrophoretic transport. In this section, we present the splitting formulation for the governing equations, and the numerical solution procedure.

1. Formulation for External Electric and Electokinetic Potential

Numerical formulation for the external electric and electrokinetic potentials are as follows:

$$\nabla^2 \phi^{n+1} = 0, \tag{3.11}$$

$$\left[\nabla^2 - \alpha\beta \cosh(\alpha\,(\psi^*)^n)\right](\psi^*)^{n+1} = \beta \sinh(\alpha\,(\psi^*)^n) - \alpha\beta\,(\psi^*)^n \cosh(\alpha\,(\psi^*)^n), \tag{3.12}$$

where n shows the iteration number, and α and β is defined in equations (3.3) and (3.4), respectively.

In the first step, Laplace equation (equation 2.7) is computed in a variational frame work to solve the electric potential for external electric field. Solution of the

Poisson-Boltzmann equation (equation 3.2) is obtained using a Galerkin projection. A Newton iteration scheme for a variable coefficient Helmholtz equation is utilized to treat exponential non-linearity in equation (3.12). The solution of a previous iteration is used for evaluation of the non-linear forcing function, and the resulting system is solved until the residual is reduced beyond a certain residual level (typically 10^{-13}). The numerical solution of Poisson-Boltzmann equation (equation 3.2) is challenging due to the *exponential non-linearity* associated with the hyperbolic-sine function and the need to resolve the electric double layer which is usually very thin compared to the bulk channel height. Especially for large values of α (in equation **??**), the non-linear forcing increases rapidly for any value of β, making the numerical solution difficult. The electroosmotic and eletrostatic potentials from this formulation will be used to obtain the electrokinetic force in the Navier-Stokes equation. The electrostatic potential will be used to calculate the electrophoretic migration velocity in the species transport equation.

2. Formulation for Navier-Stokes Equation

The splitting formulation for Navier-Stokes equation involves the following steps:

$$\tilde{\mathbf{u}} = \sum_{q=0}^{Ji-1} \alpha_q \mathbf{u}^{n-q} + \Delta t(\sum_{q=0}^{J_e-1} \beta_q \mathbf{N}(\mathbf{u}^{n-q}) + (\rho_q \mathbf{E})^{n+1}) \tag{3.13}$$

$$\frac{\partial \bar{p}^{n+1}}{\partial n} = \mathbf{n} \cdot \left[- \sum_{q=0}^{J_e-1} \beta_q \mathbf{N}(\mathbf{u}^{n-q}) - \frac{1}{Re} \sum_{q=0}^{J_e-1} \beta_q [\nabla \times (\nabla \times \mathbf{u}^{n-q})] \right] \tag{3.14}$$

$$\nabla^2 \bar{p}^{n+1} = \nabla \cdot \left(\frac{\tilde{\mathbf{u}}}{\Delta t} \right) \tag{3.15}$$

$$\nabla^2 \mathbf{u}^{n+1} - \frac{\gamma_0 Re}{\Delta t}\mathbf{u}^{n+1} = -\frac{Re}{\Delta t}(\tilde{\mathbf{u}} - \Delta t \nabla \bar{p}^{n+1}), \tag{3.16}$$

where $\mathbf{N}(\mathbf{u})$ have following relations:

$$\mathbf{N}(\mathbf{u}) = (\mathbf{u}) \cdot \nabla \mathbf{u}, \tag{3.17}$$

The electric field $\mathbf{E}$ can be obtained from the

$$\mathbf{E} = -\nabla \phi, \tag{3.18}$$

The first two steps (equation 3.13 - 3.14) are explicit and computed using the values of $\mathbf{u}$, which are computed at the quadrature points using the methods outlined in [69]. The last two steps (equation 3.15 - 3.16) are computed in a variational framework. For example, the variational statement for the pressure equation is:

Find $\bar{p} \in P^n$ that satisfies:

$$(\nabla v, \nabla \bar{p}) = -(v, \nabla \cdot (\frac{\hat{\mathbf{u}}}{\Delta t})) + (v, \frac{\partial \bar{p}}{\partial \mathbf{n}})_{\Gamma_\mathbf{u}} \quad \forall v \in P^n \tag{3.19}$$

$$\bar{p} = 0 \quad \text{on} \quad \Gamma_\mathbf{o}, \tag{3.20}$$

where $\Gamma_\mathbf{o}$ is the set of outflow boundaries, and $\Gamma_\mathbf{u}$ is the set of boundaries with specified Dirichlet velocity boundary conditions. Details on the methods used to solve the matrix systems resulting from these kind of elliptic variational statements can be found in [68]. The constants α_q, β_q in equations (3.13 - 3.14) are integration weights and they are defined in [67].

3. Formulation for Species Transport Equation

The splitting formulation for species transport equation involves the following steps:

$$\tilde{\mathbf{c}} = \sum_{q=0}^{Ji-1} \alpha_q \mathbf{c}^{n-q} + \Delta t(\sum_{q=0}^{J_e-1} \beta_q \tilde{\mathbf{N}}(\mathbf{u}^{n-q}, \mathbf{c}^{n-q})) \tag{3.21}$$

$$\nabla^2 \mathbf{c}^{n+1} - \frac{\gamma_0 Pe}{\Delta t} \mathbf{c}^{n+1} = -\frac{Pe}{\Delta t} \tilde{\mathbf{c}}, \tag{3.22}$$

where $\tilde{\mathbf{N}}$ is

$$\tilde{\mathbf{N}}(\mathbf{u}, \mathbf{c}) = (\mathbf{u} - \mu_{\mathbf{ep}} \cdot \vec{\mathbf{E}}) \cdot \nabla \theta. \tag{3.23}$$

The first step (equation 3.21) is the explicit and computed using the values of $\mathbf{c}$, which are computed at the quadrature points using the methods outlined in [69]. The last step (equation 3.22) computed in a variational framework.

Utilizing these formulations, at first, we solve the external electric potential and electroosmotic potential. Electrokinetic force is obtained from these potentials and we include it in the Navier-Stokes equation. After that, the Navier-stokes formulation and species transport formulation are solved simulaneously to obtain the velocity field and concentration field together. Spectral convergence of Poisson-Boltzmann equation in our scheme is revealed in [72] and spectral convergence of Navier-Stokes equation and species transport equation is revealed in [66].

CHAPTER IV

FLOW AND SPECIES TRANSPORT CONTROL IN GROOVED MICRO-CHANNELS USING LOCAL ELECTROKINETIC FORCES

In this chapter, we present numerical simulation results for flow and species transport control in grooved micro-channels using locally applied electric fields, and zeta potential patterned groove surfaces. The resulting mixed electroosmotic/pressure driven flow enables entrapment and release of prescribed amounts of scalar species in the grooves. We demonstrate that the groove size and shape determine volume of the entrapped species, and depending on the local electric field and zeta potential, each groove can simultaneously contain up to two species. This framework allows control over the inter-species diffusion and mixing using simple flow kinematics, and it is easily applicable for electrically neutral species. We envision utilization of this technique for combinatorial chemistry experiments in a micro-channel with multiple grooves, where each groove can be addressed (filled, emptied or mixed) independently.

A. Introduction

Electroosmosis enables fluid pumping and flow control using external electric fields, eliminating the need for mechanical pumps or valves with moving components. Comparisons between the electroosmotically and pressure-driven flows reveal several important differences. First, the volumetric flowrate (per channel width) in electroosmotic flows varies linearly with the channel height (h), enabling useful flowrates in micro-channels and nano-channels with low driving electric fields. However, the flowrate (per unit width) in pressure-driven flows vary as cube of the channel height (h^3). This requires unrealistically large pressure drops, making pressure-driven flows impractical for nano-channel applications. Second, the velocity profiles for electroos-

motic flows are (mostly) uniform (plug-like), while the pressure driven flow velocity profiles are parabolic. This difference has significant effects in species transport and dispersion in micro-fluidic applications.

Utilization of local electroosmotic forces for flow and species transport control require selectively applied electric fields, and modifications of the surface charge in certain portions of the flow domain. Local electric fields can be applied using patterned electrodes [74], while the alteration of surface charge can be obtained by either static or dynamic polymer coatings. The static coating is based on covalent bonding between the coating material and capillary surface, but dynamic coating relies on the ionic interactions [29, 30]. Dynamic coating is an active field of research. Using different polymer bilayers, such as cationic layer of polybrene and anionic layer of dextran sulphate, it was possible to change the direction and magnitude of the flow [31]. Both of these coatings reproduced electroosmotic flow for a wide range of pH values. It is also possible to suppress electroosmotic flow. Kaniansky and co-workers worked on eight different electroosmotic flow suppressors and have shown influences of these on electrophoretic separation efficiencies at different pH values [32], while Ramsey and co-workers suppressed electroosmosis using poly-dimethylacrylamide [33]. Barker *etal.* have used polyelectrolyte multilayers to alter the electroosmotic flow direction in polystyrene and acrylic micro-fluidic devices [34].

Embedded surface electrodes can also be utilized to locally alter the zeta potential. Schasfoort *etal.* have built micro-channels using a conducting material, and have covered these with a thin layer of insulator. They have shown modification of the surface charge and the resulting electroosmotic flow by applying an electrostatic potential on the insulator covered electrodes [74]. A similar approach for direct zeta potential control has also been implemented in [36]. These developments enable alterations of the surface characteristics at will. This can also result in *time-dependent*

alteration of the zeta potential.

The objective of this chapter is to demonstrate flow and species transport control using locally applied electric fields, and zeta potential patterned surfaces in grooved micro-channels. The grooved channel is a well known test-bed, which exhibits flow recirculation even in the Stokes flow regime, where the Reynolds number $Re \rightarrow 0$. The fluid entrapped in the recirculation zone can not be released without any external forces. However, this geometry can be useful for micro-fluidic applications, if we can selectively and locally alter or eliminate these separation zones using the electrokinetic forces. We envision at least two applications for this flow control scheme. The first one is heat transfer enhancement in micro-electronic cooling, where addition of the grooves increase the surface area, and elimination of the recirculation regions that entrap high temperature fluid increases convective heat transfer from the groove surface. The second application is design of a serial micro-fluidic process, where we entrap and release *prescribed* amounts of *multiple species* in a micro-channel with multiple grooves. The groove size determines volume of the entrapped species. In addition, each groove can simultaneously contain up to two species, allowing control over the inter-species diffusion and mixing by simple flow kinematics. Such devices can be utilized for combinatorial chemistry experiments in a micro-channel.

Motivated by these applications we investigate the mixed electrokinetic/pressure driven flows in grooved micro-channels with zeta potential patterned side surfaces. The flow geometry is schematically shown in Fig. 3. The electric field is applied across the channel using the top and bottom surface electrodes. This induces local electrokinetic forces on the side surfaces that enable flow control, while the flow in the main channel is maintained by a pressure drop.

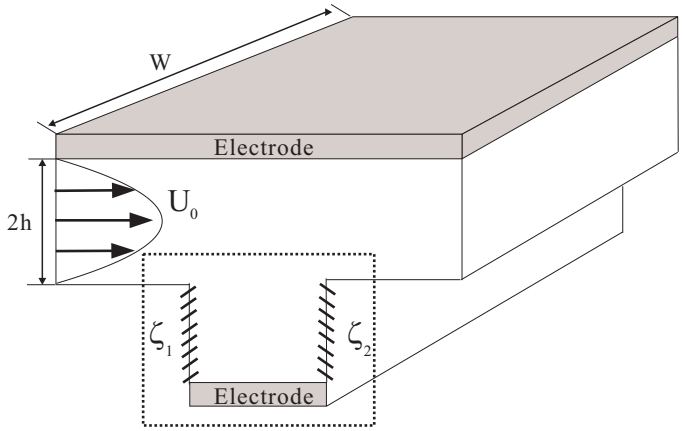

Fig. 3. Schematic diagram for the grooved channel geometry with zeta potential patterned side surfaces. The top and bottom surfaces are made out of an electrode material, which enables a locally applied electric field in the vertical direction. The dotted line region enclosing the groove section indicates the plot domain for Figs. 4-12.

B. Flow Control in Grooved Micro-Channels

In this section we present the basic flow patterns and streamlines obtained in a grooved-channel under local electrokinetic forces. In order to evaluate these *local effects*, we first present in Fig. 4-a the streamline patterns in a pressure driven viscous flow at $Re = 0.02$. The flow pattern, obtained using two-dimensional simulations exhibits a recirculation zone in the groove. This is also an expected result for three-dimensional grooved-channels, where the channel width W is much larger than the channel height $2h$ (Fig. 3). Otherwise, the separation regions will be reduced or annihilated due to the Hele-Shaw type flow.

Electroosmotic (EO) flow in a constant ζ potential channel, driven by a streamwise electric field is significantly different than the pressure driven viscous flow. In absence of externally applied pressure gradients, pure EO flow in a grooved channel does not exhibit any recirculation zones, as shown in Fig. 4-b. Details of this flow,

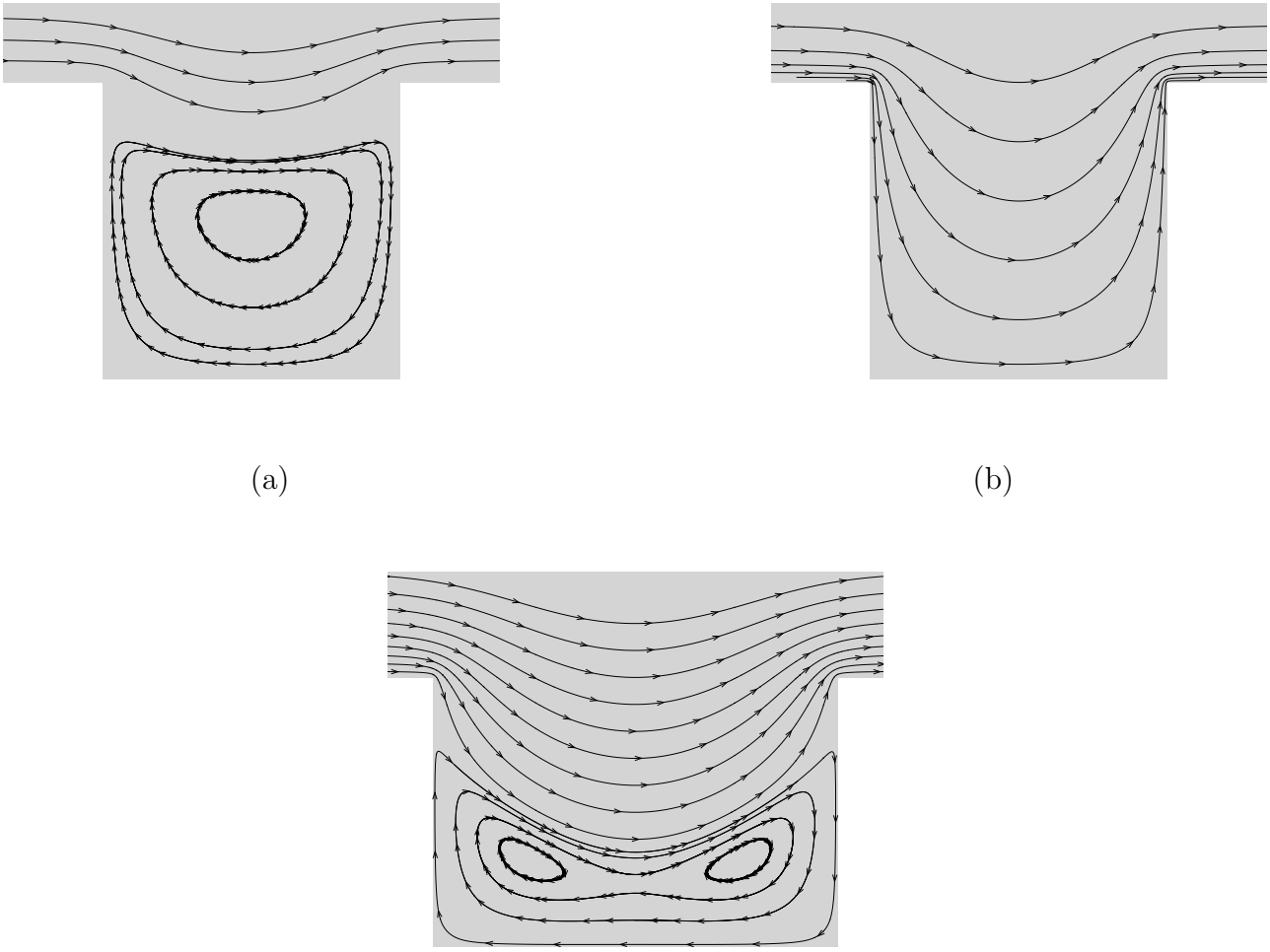

(a) (b)

(c)

Fig. 4. Classical flow patterns obtained in a square grooved channel: Pressure driven flow (a), and pure electroosmotic flow under constant zeta potential and streamwise electric field (b). Pressure driven Stokes flow in a 1 : 1.5 aspect ratio rectangular groove channel (c).

and point-wise comparisons between the numerically predicted and experimentally measured velocity profiles in a grooved micro-channel were presented in [21]. Since the pure EO flow in Fig. 4-b is generated by an external electric field, and it does not allow flow control in channels with multiple grooves, unless the ζ potential on groove surfaces can be altered at will, in a time dependent fashion. Experimental demonstrations of ζ potential alterations at will were presented in [74]. However, design of such a flow system can be quite cumbersome.

In the rest of this section, we present the streamline patterns obtained by locally applied electric fields, and zeta potential patterned surfaces in grooved microchannels. We performed systematic studies by modifying the groove geometry, polarity and the magnitude of the externally applied electric field, and the ζ potential. We will investigate four different cases shown in Fig. 5. The ζ potential and direction of the electric field for each case are shown on the figure. Once the ζ potential of each surface is fixed, we can alter between the cases 1 and 2, as well as cases 3 and 4, simply by reversing the electrode polarity. This is a more convenient method for flow control than changing the zeta potential.

In simulations, the relative importance of electroosmotic and hydrodynamic velocities are represented by u_{HS}/u_o, where u_o is the characteristic hydrodynamic velocity at the center of the channel. Following equation (2.14), it is possible to adjust u_{HS} by varying the zeta potential via surface patterning, changing the buffer concentration and pH, and also by varying magnitude of the externally applied electric field. Although increasing the applied electric field is quite convenient, it has several *practical limitations*, such as the electrolysis of water, Joules heating, electrode oxidation, and possible pH fluctuations in the system. Therefore, actual implementation of the control process requires careful considerations of these limitations.

In micro-flows, the Reynolds number (Re) that determines the relative impor-

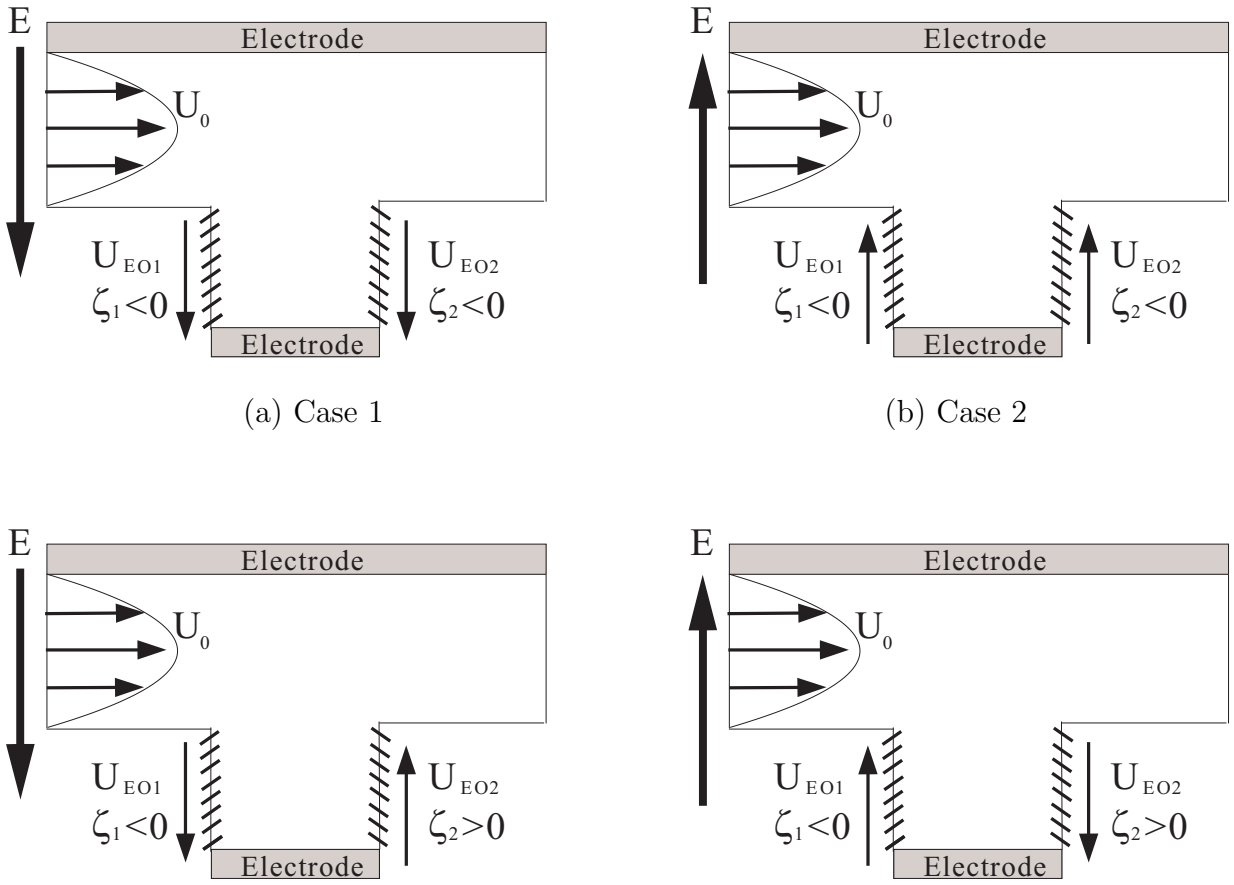

(a) Case 1

(b) Case 2

(c) Case 3

(d) Case 4

Fig. 5. Schematic diagram for the grooved channel geometry with zeta potential patterned side surfaces. Polarities of the electric field and the zeta potential on the side surfaces are shown along with the local electroosmotic flow direction.

tance of inertial to viscous forces, is often very small ($Re << 1$). Therefore micro-flows are usually in the Stokes flow regime. This is an advantage for flow control in micro-systems, since the Stokes flow velocity field is often *insensitive* to the variations in Reynolds number. Insensitivity of the flow field to Reynolds number makes the following results, obtained at $Re = 0.02$, uniformly valid in the entire Stokes flow regime ($Re < 1$). An important implication of this for flow control is that all u_{HS}/u_o ratios utilized in this study can be observed in actual experiments. For example, flow of deionized water ($c_o = 1 \times 10^{-6} M$) in glass channels ($\zeta \simeq -25.4mV$) results in $u_{HS} = 0.67mm/s$ at $E = 37V/mm$. In a micro-channel with characteristic dimension of $h = 30\mu m$, this results in $Re = u_{HS}h/\nu = 0.02$. If we choose to base Re on u_o, the same Reynolds number will be obtained using $u_o = 0.67mm/s$. At this point, $u_{HS}/u_o > 1$ cases can be obtained by reducing u_o, while keeping u_{HS} a constant. Similarly, the $u_{HS}/u_o < 1$ cases can be obtained by reducing the u_{HS} while keeping u_o constant. Either approach maintains Stokes flow conditions for a wide range of physical parameters.

1. Square Groove

We first investigate flow control in a square-groove, where the groove step height and length are equal to the main channel height. In Fig. 6 (top row), we show the streamlines obtained as a result of case 1 in Fig. 5-a. Only the right portion of the groove has a recirculation zone, while the left portion sweeps the fluid. This flow pattern enables species entrapment in the recirculation region of the groove, which can be controlled by changing the magnitude of the electric field. For example, the recirculation zone covers about half of the groove, when $u_{HS}/u_o = 1.0$. However for smaller u_{HS}/u_o ratios the recirculation zone is larger. For zero external electric field, the flow recovers the classical Stokes flow pattern shown in Fig. 4-a. Reversing the

electric field direction in case 1, we obtain the case 2 (Fig. 5-b). The streamline patterns obtained for this case are presented in Fig. 6 (bottom row). This creates recirculation zones in the left side of the groove, which are mirror-images of the flow patterns observed in case 1.

Cases 3 and 4 require surface patterning shown in Figs. 5-c and -d. For case 3, the electric field is downwards. Consequently, the electroosmotic flow direction is upwards for the right side of the groove, while it is downwards for the left side. The resulting streamline patterns are shown in Fig. 7 as a function of the u_{HS}/u_o ratio. Starting from the pure Stokes flow pattern of Fig. 4-a, $u_{HS}/u_o = 0.01$ results in three distinct recirculation zones. This demonstrates sensitivity of the flow to local electroosmotic effects. Small increases in u_{HS}/u_o result in quite different flow patterns. For example, the $u_{HS}/u_o = 0.05$ case has three recirculation zones. However, the primary recirculation zone in the middle of the groove is significantly weaker for $u_{HS}/u_o = 0.05$ compared to the $u_{HS}/u_o = 0.01$ case. Increasing the u_{HS}/u_o ratio to 0.1 completely eliminates the recirculation regions in the groove, resulting in flow patterns qualitatively similar to that of pure electroosmotic flow, shown in Fig. 4-b. Further increase in the u_{HS}/u_o ratio (as shown for the 0.5 case) pulls more streamlines into the groove. Since path-lines of noninertial particles will follow the streamlines in steady flow, we can pull in more streamlines (and fluid particles) towards the groove simply by adjusting the electric field. This enables further possibilities for flow and species transport control, since one can vary the portion of the bulk flow region that interacts with the groove section, simply by adjusting the external electric field magnitude.

Reversing the electric field direction of case 3, we obtain case 4 shown in Fig. 5-d. Increasing the u_{HS}/u_o ratio enhances the recirculation zones, as shown in Fig. 8. This flow pattern is important, since it enables efficient capture of electrically neutral

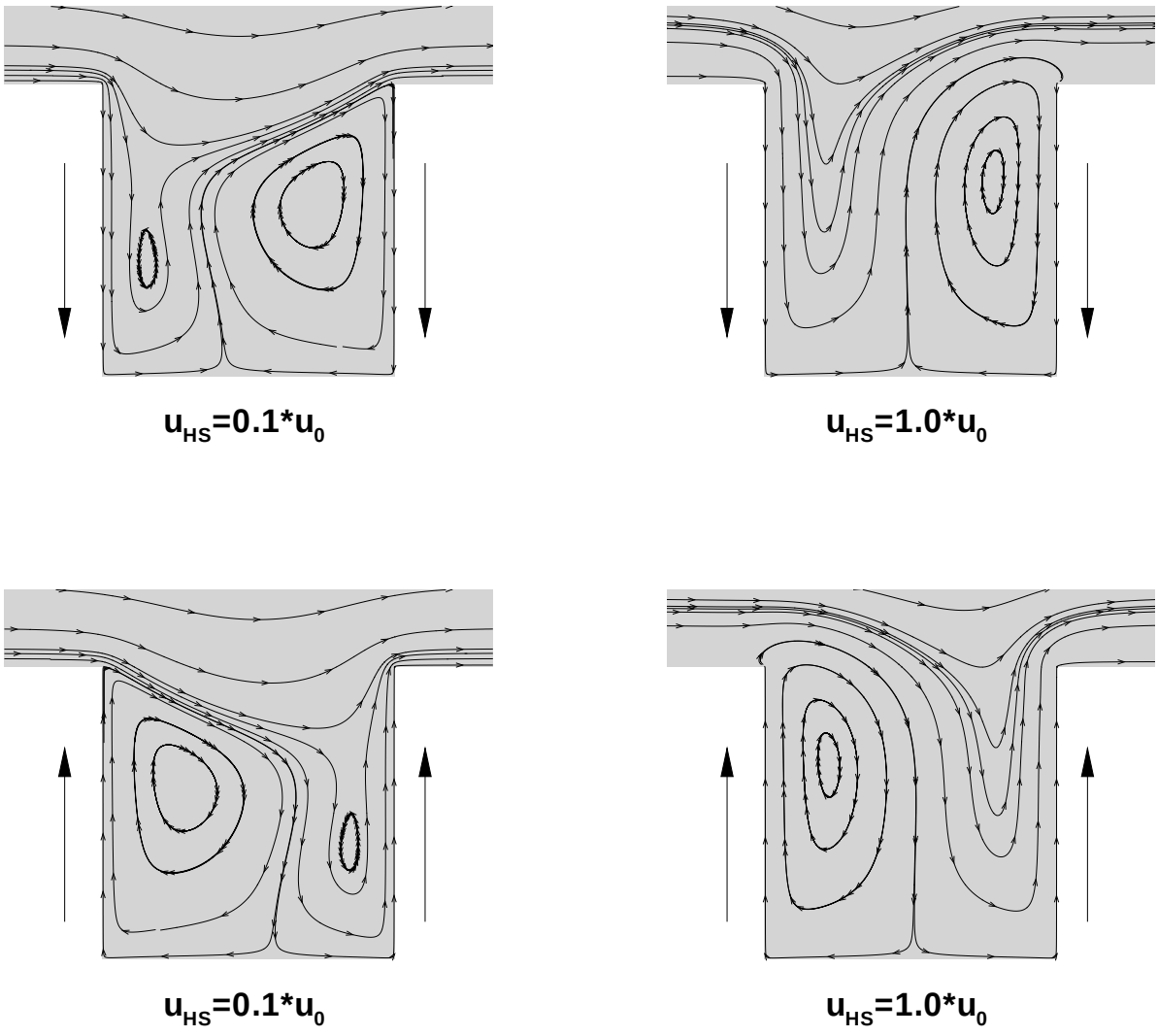

Fig. 6. Streamlines for the square groove for cases 1 and 2 (Top, and bottom rows, respectively) under various u_{HS}/u_o conditions (see Fig. 5-a and -b)

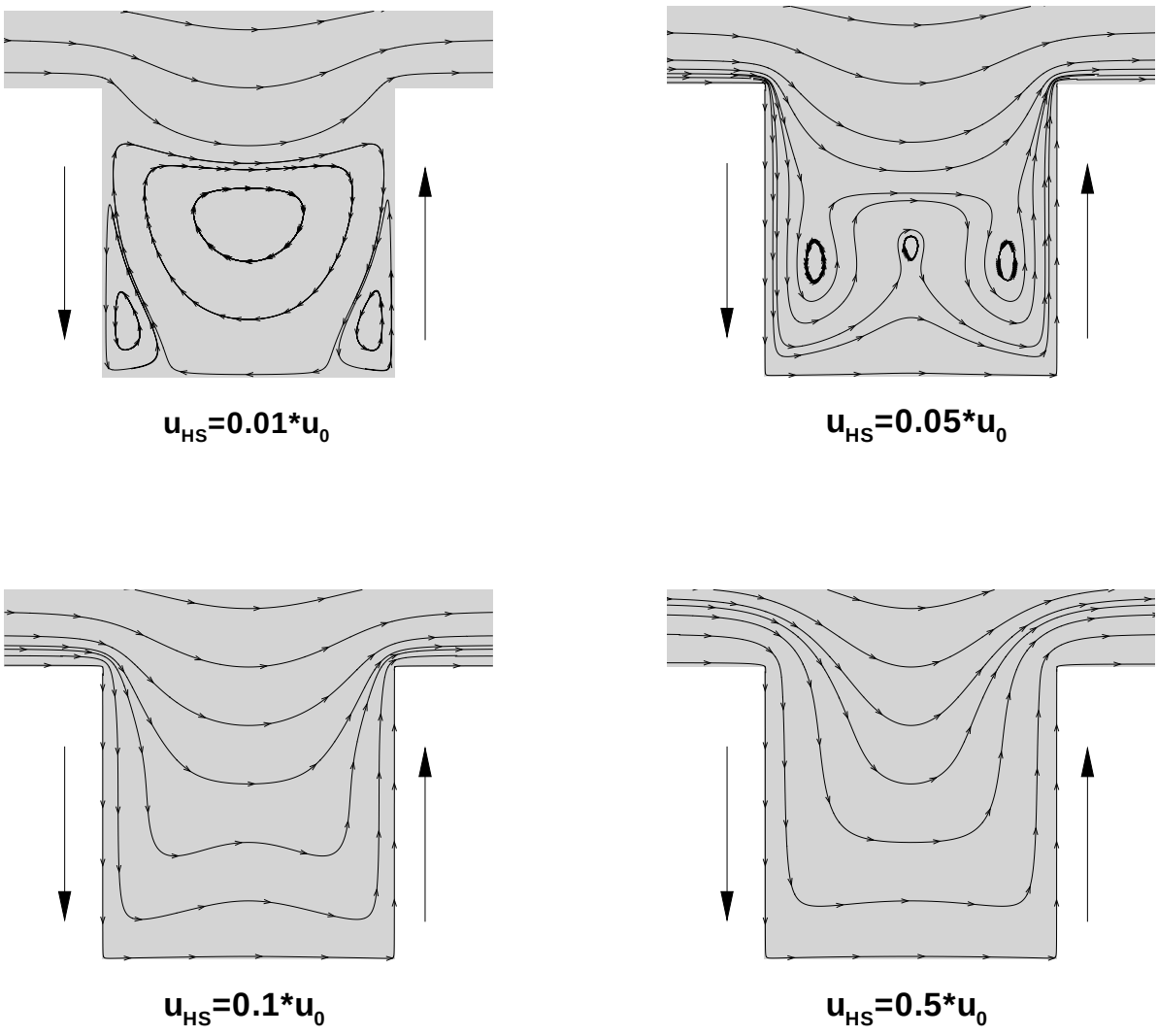

Fig. 7. Streamlines for the square groove for case 3 (see Fig. 5-c) under various u_{HS}/u_o conditions.

species. Comparing the streamline patterns in Fig. 8 with that of the pressure driven Stokes flow in Fig. 4-a, we observe that case 4 at $u_{HS}/u_o = 0.5$ enables entrapment in the entire groove.

2. Rectangular Groove and Other Geometric Effects

In the previous section we investigated the square-groove geometry. In order to demonstrate the sensitivity of flow patterns to the geometry, we investigate flow control in a rectangular groove with $1 : 1.5$ groove-side to length ratio. The numerical experiments are based on the four cases shown in Fig. 5. The groove aspect ratio affects the number and size of the recirculation zones. In Fig. 4-c we present streamlines for Stokes flow in absence of electrokinetic effects. We observe two recirculation zones as a result of the increased aspect ratio. Further increase in the channel aspect ratio reduces the recirculation regions. However circulation regions are observed on both surfaces even for very low Reynolds number flows [75].

Flow patterns corresponding to case 1 are shown in Fig. 9. Increasing the u_{HS}/u_o ratio, we observe significant changes in the streamline patterns as demonstrated by comparison between the $u_{HS}/u_o = 0.01$ and 0.02 cases. Further increase in the u_{HS}/u_o ratio results in flow patterns qualitatively similar to the square groove geometry. Reversing the electric field direction results in case 2. The streamline patterns for this case are shown Fig.10. Similar to the square-groove geometry, we observe reversal in the flow pattern, when we reverse the electric field.

For case 3, we observe transition between two recirculation zones of the pure Stokes flow to elimination of the recirculation zones with increased u_{HS}/u_o ratio. However, this transition happens rather interestingly (Fig. 11). At $u_{HS}/u_o = 0.01$ we observe four recirculation zones. This drastically changes at $u_{HS}/u_o = 0.02$, and the separation zones are eliminated at $u_{HS}/u_o = 0.06$. For case 4, we observe double

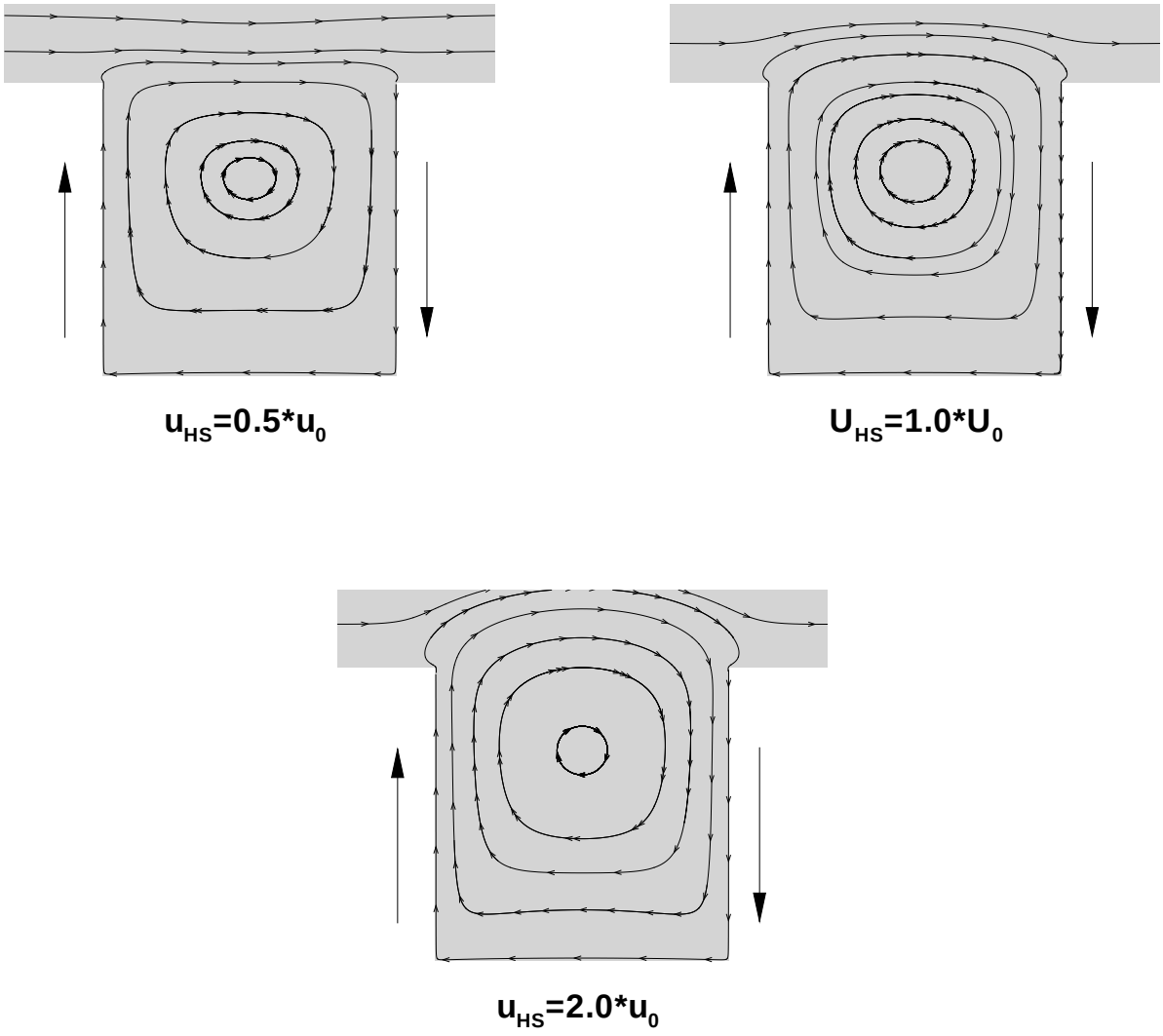

Fig. 8. Streamlines for the square groove for case 4 (see Fig. 5-d) under various u_{HS}/u_o conditions.

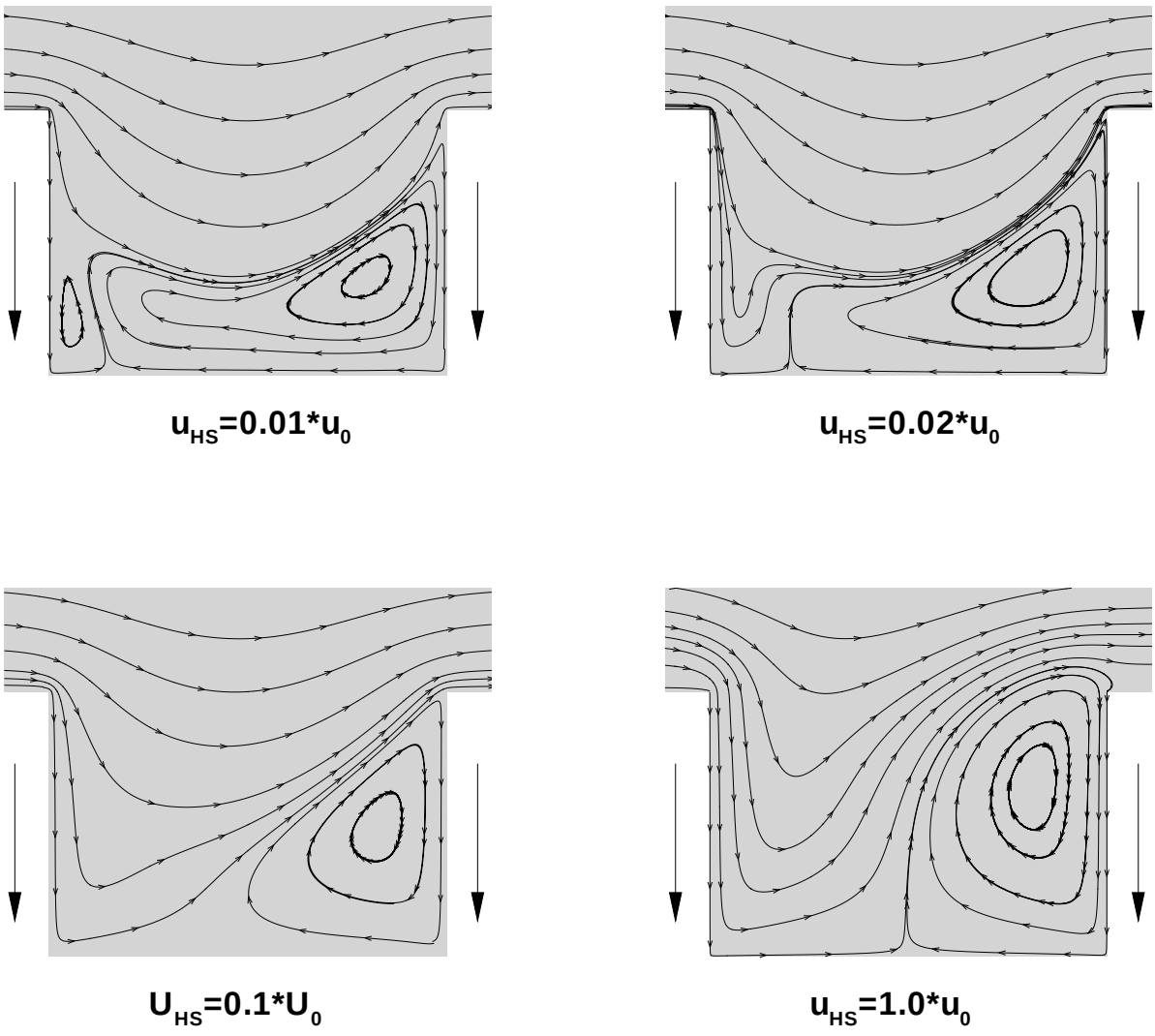

Fig. 9. Streamlines for the 1 : 1.5 aspect ratio rectangular groove for case 1 (see Fig. 5-a) under various u_{HS}/u_o conditions.

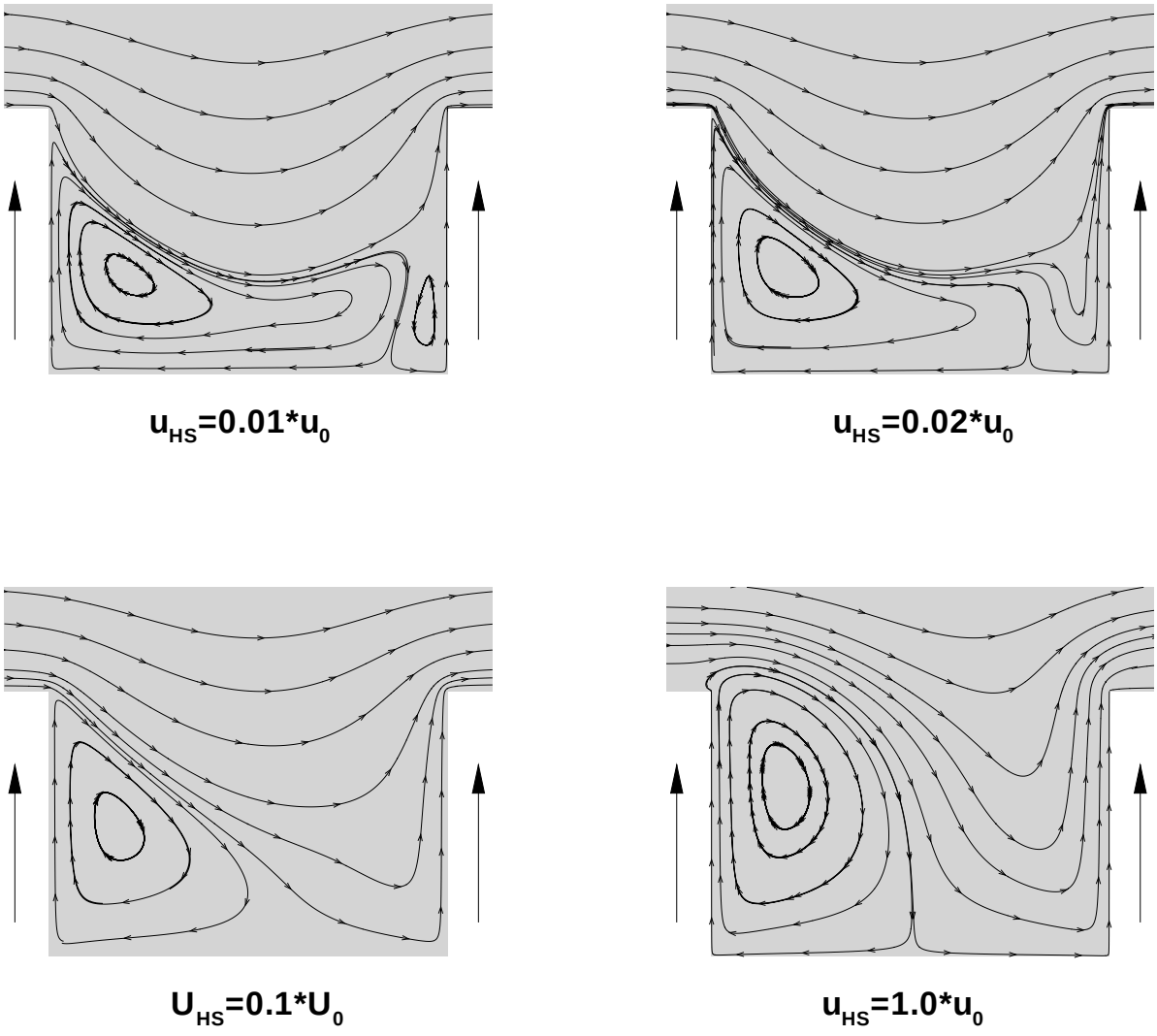

Fig. 10. The streamlines for the $1:1.5$ aspect ratio rectangular groove for case 2 (see Fig. 5-b) under various u_{HS}/u_o conditions.

recirculation zone in the groove, whose size and location depend on the magnitude of the electrokinetic force (Fig. 12). Compared to the square groove, the $1:1.5$ aspect ratio rectangular groove is more sensitive to the locally applied electrokinetic forces.

In Figs. 13-a and -b, we present a systematic study of geometric effects by comparing case 3 flow pattern in square, and $1:1.5$ aspect ratio rectangular grooves. The electric field and zeta potential of the side surfaces obey case 3 shown in Fig. 5-c. In the following, we deliberately utilized $u_{HS}/u_o = 5$ to demonstrate formation of rather counter-intuitive flow patterns. Unlike the previously shown $u_{HS}/u_o \leq 1$ cases, a new recirculation pattern emerges in the groove, while the channel top surface experiences first adverse and then favorable pressure gradients, evident from the streamline patterns. Further increasing the groove aspect ratio, the step expansion and sudden contraction regions do not interact any more, and we obtain classical problems of the backward and forward facing step geometries. The backward facing step geometry with channel-inlet height to step height ratio of 1 exhibits a small separation region even at $Re = 0.02$ [75]. In Figs. 13-c and -d, we show the flow patterns obtained by an upwards electroosmotic velocity of $u_{HS}/u_o = 5$ and downwards electroosmotic velocity of $u_{HS}/u_o = 7$, respectively. For both of these cases only the step-surface has finite zeta potential, and the electric field is applied vertically to create an upward or downward electroosmotic force. Fig. 13-c shows enhanced separation region near the step expansion, as expected. Fig. 13-d shows two recirculation regions as a result of the strong downward momentum imposed by the electroosmotic velocity near the surface, which diverts rather weaker flow in the main channel towards the bottom wall. This creates adverse pressure gradients on the top surface, and leads to a second separation zone on the top wall. Further increase in the downward electroosmotic velocity ($u_{HS}/u_o = 10$) results in merging of these two recirculation sections to one large recirculation bubble.

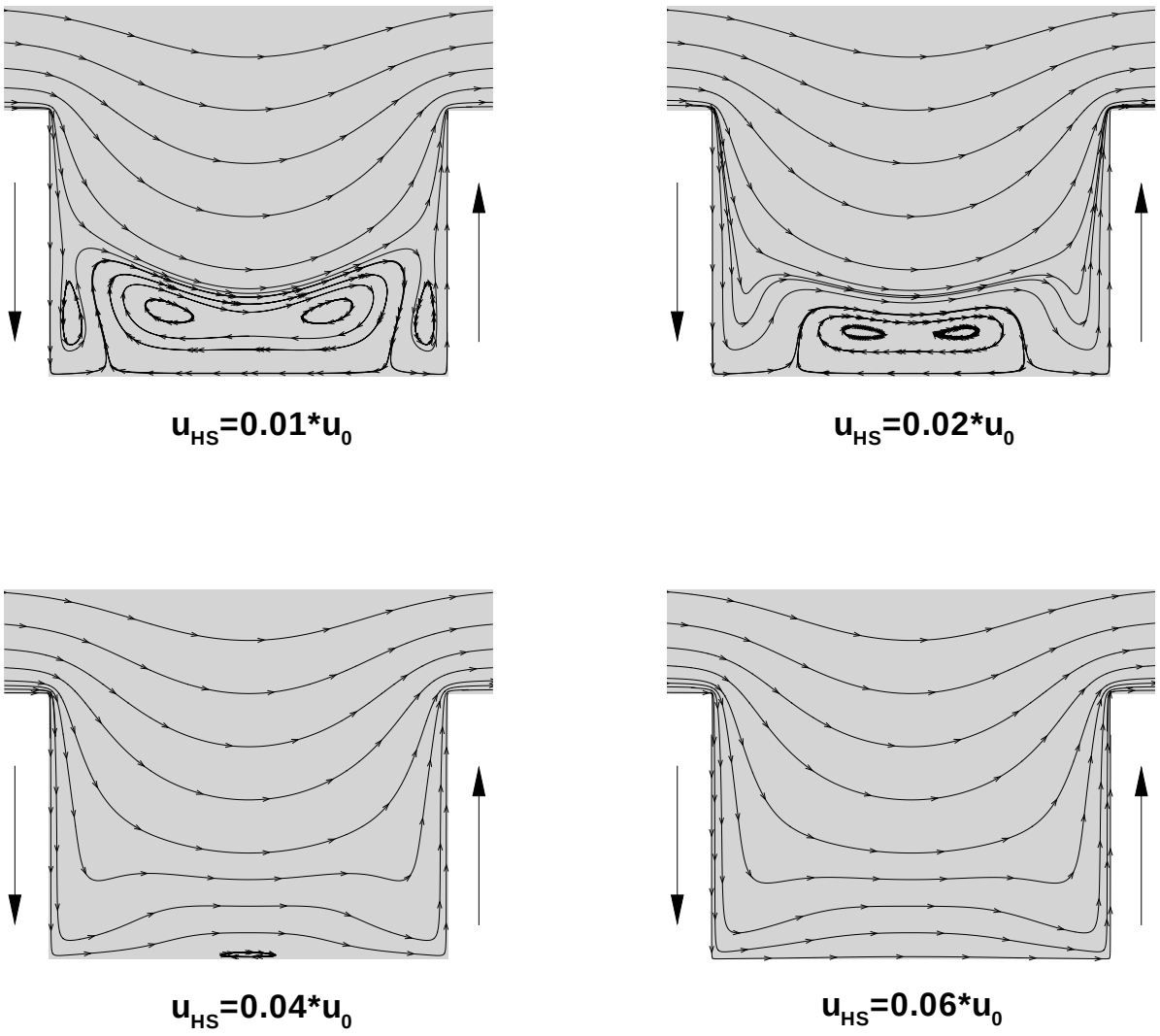

Fig. 11. Streamlines for the $1:1.5$ aspect ratio rectangular groove for case 3 (see Fig. 5-c) under various u_{HS}/u_o conditions.

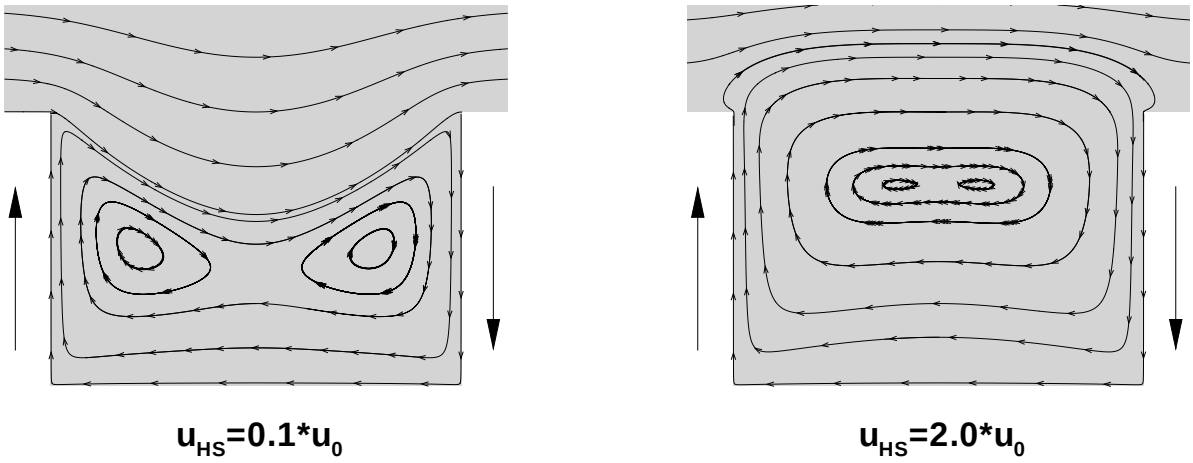

Fig. 12. Streamlines for the $1:1.5$ aspect ratio rectangular groove for case 4 (see Fig. 5-d) under various u_{HS}/u_o conditions.

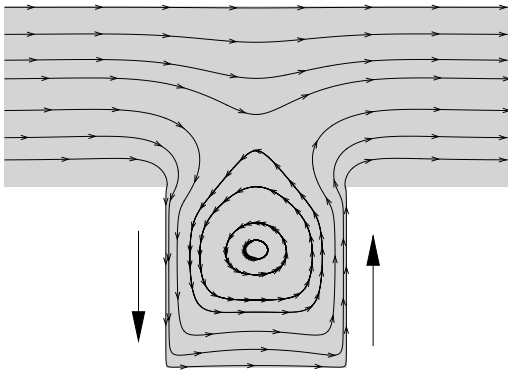

$u_{HS}=5.0*u_0$

(a)

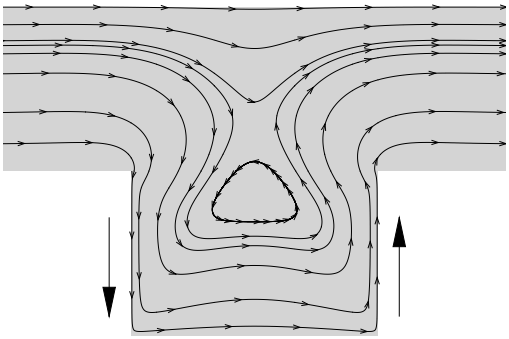

$u_{HS}=5.0*u_0$

(b)

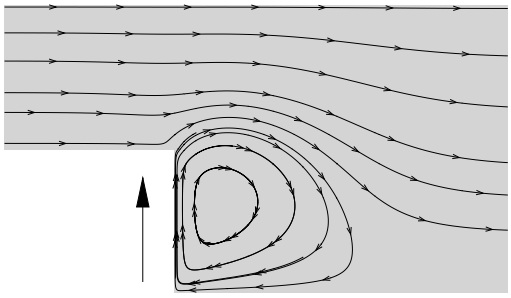

$u_{HS}=5.0*u_0$

(c)

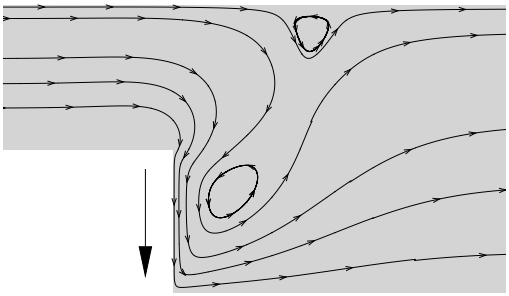

$u_{HS}=7.0*u_0$

(d)

Fig. 13. Flow patterns at large u_{HS}/u_0 ratios in square groove (a); 1 : 1.5 aspect ratio rectangular groove (b); backward facing step with upwards (c) and downwards (d) electroosmotic flow.

C. Species Transport Control

In this section we demonstrate species transport control by capture and release of electrically neutral species in the square-grooved channel. Flow control for charged species requires consideration of their electrophoretic mobility. Since the electrophoretic transport is proportional to the local electric field (equation 2.16), this is an additional effect that needs further considerations in addition to the combined viscous and electroosmotic flow effects. Therefore, flow /transport control for charged species requires mobility specific modifications of the flow control scheme. For this reason, we will present species transport control for electrically neutral species only. Our objective is to demonstrate the feasibility of a serial micro-fluidic process, where we entrap and release *predetermined* amounts of tagged fluid particles (species) in a grooved micro-channel.

Particularly we consider two electrically neutral miscible fluids with identical densities. The first species (A) is tagged with a marker (such as a dye), while the second species (B) is untagged. In the species transport simulations we specify the Helmholtz-Smoluchowski slip velocity on groove side boundaries. Unlike in the previous section, the EDL is not resolved. This significantly reduces the computational time. All simulations are performed for $u_{HS}/u_o = 1$. The Reynolds number based on the average channel velocity and half channel height is $Re = 0.005$. Despite the very low Re, we imposed Peclet number $Pe = 1,000$, which corresponds to $Sc = 2 \times 10^5$. Such large Schmidt numbers are typical of large particles suspended in aqueous solutions, as often observed in flow-tracing dyes, and bio-molecules [76].

First, we fill the groove with species A using case 3, shown in Fig. 5-c. Then we reverse the polarity of the electric field to obtain case 4 corresponding to Fig. 5-d. Case 4 traps species A in the groove section, while we flow species B through the

channel using a pressure driven flow. We show snapshots of this process in Fig. 14 (a-f) at different times, where t^* is the non-dimensional time based on the convective time scale (h/u_{HS}). This demonstrates species entrapment in the groove despite the pressure driven flow in the channel. We note that the groove size determines volume of the entrapped species. It is possible to *sequentially entrap* several different species using flow patterns of cases 3 and 4 in a long micro-channel with multiple grooves.

After the entrapment process, we demonstrate species release in absence of the driven flow. For this we utilized the electric field and zeta potential of case 4, which induces larger recirculation zones that penetrate towards the middle of the channel.

The concentration contours obtained during this process are shown in Fig. 15. The flow field of case 4 creates a rather unique effect in absence of pressure driven flow. Species A levitates towards the middle of the channel by a clock-wise rotation, which also entrains species B into this circulation zone. As a result, we observe weak convective/diffusive mixing between the two species. This method may allow control over the inter-species diffusion and mixing based on the Peclet number and the time of application of this flow pattern.

Once the species are levitated, we turn on the pressure driven flow and change polarity of the electric field, to induce flow pattern of case 3. This results in release of the species as shown in Fig. 16 (a-f). We must note that the levitation step is unnecessary to release the entrapped species from the grooves. In Fig. 16 we observe rapid release of the species by pressure driven flow.

It is also possible to trap two separate species in a single groove simultaneously. In order to demonstrate this, we first fill the entire channel with species A. Then we turn on the electric field to create the flow pattern of case 1 (Fig. 5-a), while we pump species B through the channel. This traps species A in certain portion of the groove, while the rest of the groove is filled with species B, as demonstrated in the

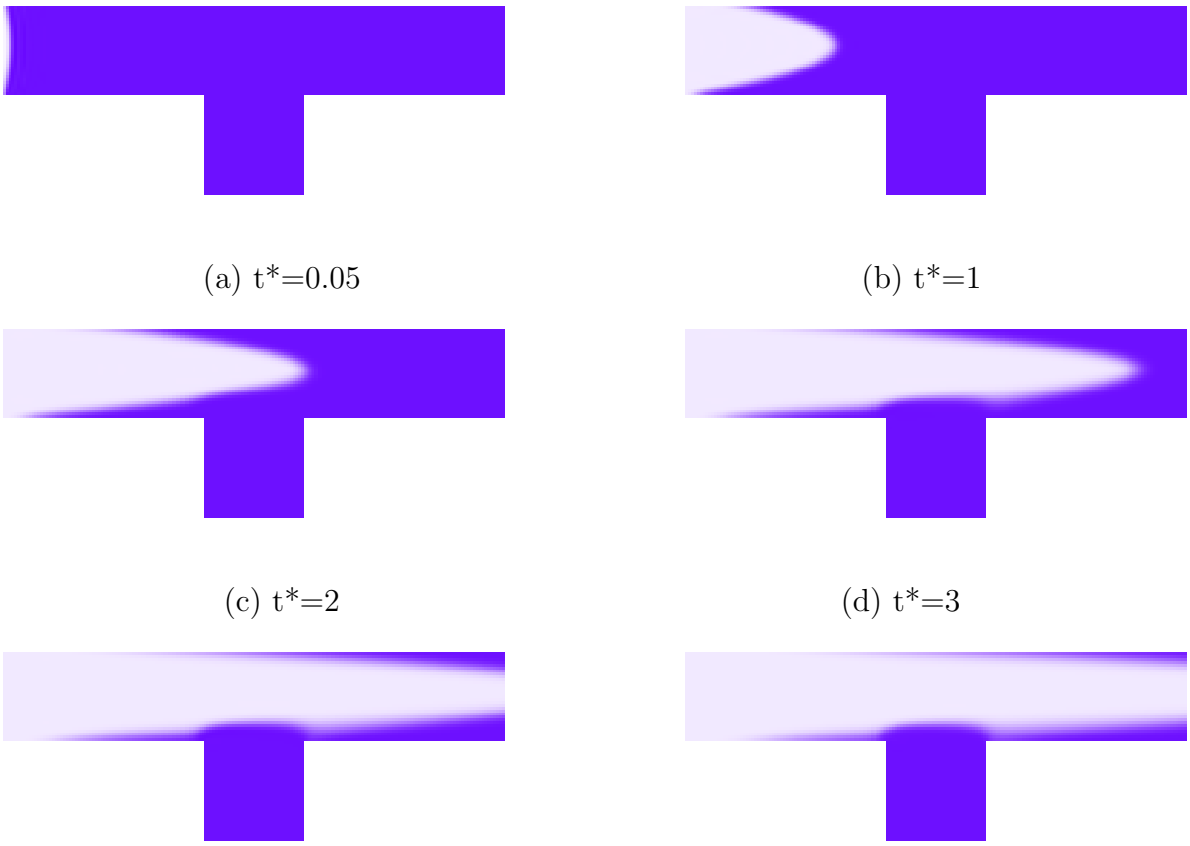

(a) t*=0.05 (b) t*=1

(c) t*=2 (d) t*=3

(e) t*=4 (f)t*=5

Fig. 14. Snapshots of concentration contours during entrapment of species A in the groove using case 4 (Fig. 5-d), while the species B is flowing in the channel. Time t^* is normalized by the convective time-scale: h/u_{HS}. Simulation results are obtained for $Re = 0.005$ and $Pe = 1,000$.

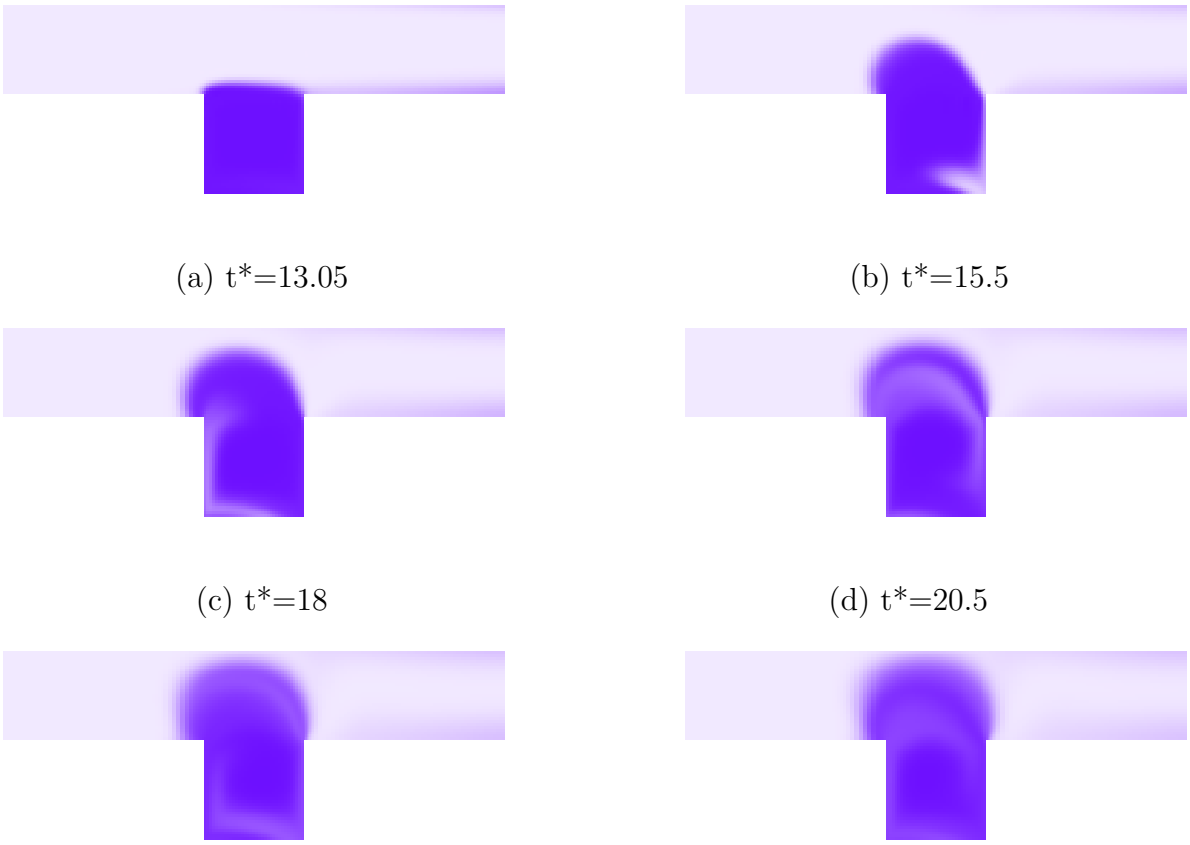

(a) t*=13.05 (b) t*=15.5

(c) t*=18 (d) t*=20.5

(e) t*=23 (f) t*=25.5

Fig. 15. Snapshots of concentration contours demonstrating levitation of the entrapped species A using control pattern of case 4 without the pressure driven flow.

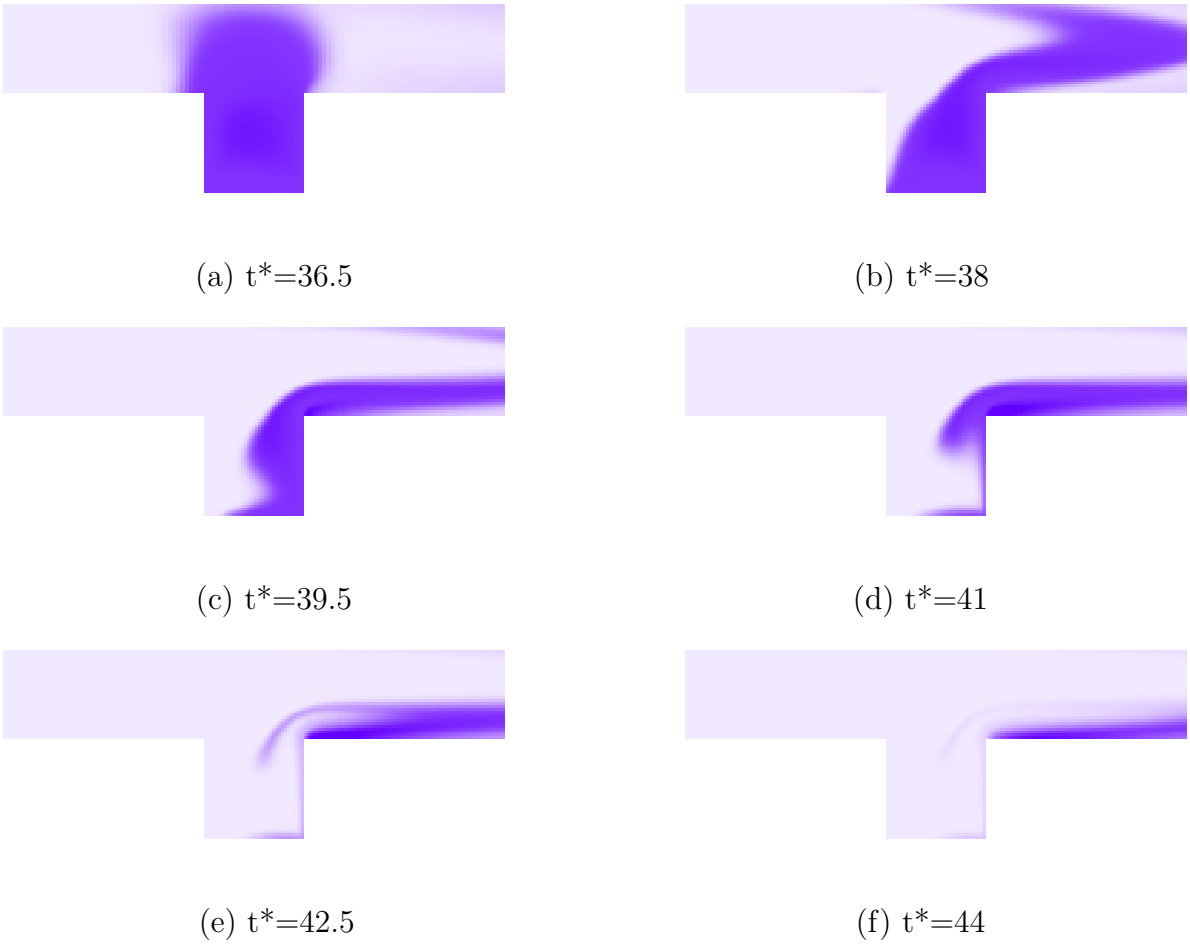

(a) t*=36.5 (b) t*=38

(c) t*=39.5 (d) t*=41

(e) t*=42.5 (f) t*=44

Fig. 16. Snapshots of species release, obtained using the flow control pattern of case 3 (Fig. 5-c).

snapshots of Fig. 17 (a-f).

D. Discussions

We demonstrated flow control concepts in a grooved micro-channel using selectively patterned, electroosmotically active surfaces and locally applied electric fields. This framework enables formation of rather complex flow patterns in simple micro-geometries. Ability to vary the electric field magnitude and its polarity also manifests time-dependent flow alterations, which results in flow and species transport control abilities. The results obtained in a single micro-groove constitute the proof of concept for flow and species transport control in an integrated serial micro-fluidic process, where *multiple species* can be trapped and released in *prescribed* amounts in a micro-channel with multiple grooves. The groove size determines volume of the entrapped species. In addition, each groove can simultaneously contain one or two species at the same time. The proposed flow and species transport control scheme allows control over the inter-species diffusion and mixing time and length scales by simply adjusting the electric field direction and its magnitude.

Extension of the proposed method for electrically charged species requires considerations of the electrophoretic mobility of each species, where the combined hydrodynamic/electroosmotic velocity should overwhelm the local electrophoretic velocity. Therefore, design of a practical device to capture and release charged species would require a priory knowledge of the electrophoretic mobility of these species. Demonstration of charged species control in complex geometries will be reported in future studies.

Finally, fabrication of large aspect ratio ($W >> h$) grooved channels with selective electrode and zeta potential patterned surfaces shown in Fig. 3 may require

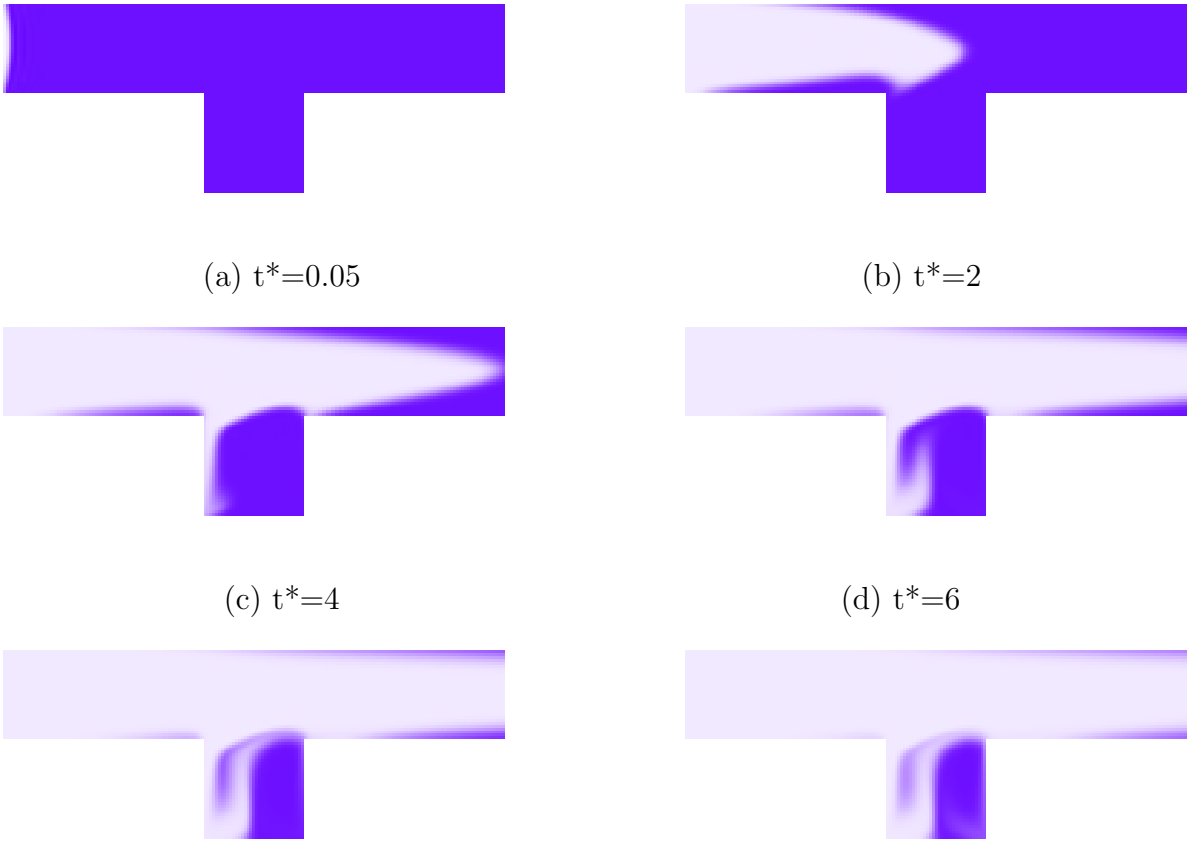

(a) t*=0.05 (b) t*=2

(c) t*=4 (d) t*=6

(e) t*=8 (f) t*=10

Fig. 17. Demonstration of simultaneous entrapment of two species in the groove, obtained using the flow pattern of case 1 (Fig. 5-a).

several processes that include micro-scale CNC machining, followed by the assembly of several interconnecting parts, and packaging.

CHAPTER V

ON-CHIP MULTI-SPECIES DETECTION USING HYDRODYNAMIC/ELECTROKINETIC FOCUSING

In this chapter we present a new microfluidic device concept for electrophoretic mobility and (relative) concentration measurements of dilute mixtures. The device enables *stationary focusing points* for each species, where the species convection velocity is zero. Simultaneous measurements of the electroosmotic mobility of an electrically neutral specie can be utilized to calculate the electrophoretic mobility of charged species. This leads to identification of the species in the mixture and we can detect multiple species in dilute mixtures.

A. Basic Features

The basic design, shown in figure 18, consists of multiple parallel channels that gradually expand to the main channel downstream of the device. We have chosen the inner-channel half height h_o and length L_0. In this schematics and the following numerical simulations, we have utilized 5 progressively expanding channels with half height of h_i, $i = 1, ..., 5$. Each inner channel is ΔL longer than the previous channel ($L_i = L_{i-1} + \Delta L$), and the main channel length is L_5. In the following, we will ignore the individual channel thickness, and their effects on the flow and electric fields for simplicity.

1. Hydrodynamic Flow

All channels on left side of the device are closed, with the exception of the inner channel that is connected to a syringe pump, where a pressure driven flow with flowrate $\dot{Q}$ is imposed from left to right. The channel width W (into the page direction

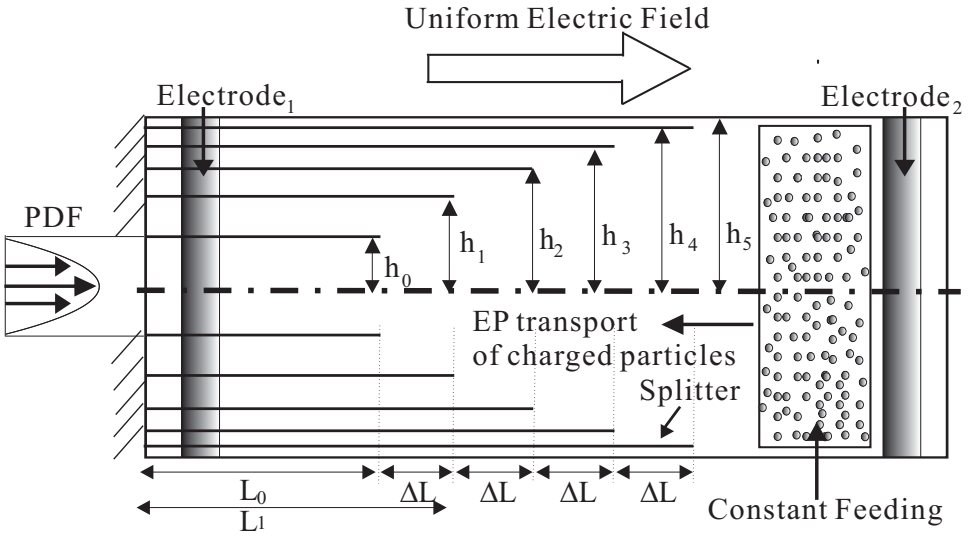

Fig. 18. Schematic view of the new mobility measurement device

in figure 18) is assumed much larger than the maximum channel height h_5, so that neglecting the boundary layer effects from the top and bottom surfaces of the device, we approximate the flow as two-dimensional. Therefore, the volumetric flowrate per channel width is

$$\dot{q} = \frac{\dot{Q}}{W}, \tag{5.1}$$

while the channel averaged hydrodynamic velocity ($\bar{u}_i$) in each channel becomes

$$\bar{u}_i = \frac{\dot{q}}{h_i}, \tag{5.2}$$

Using this one-dimensional analysis, we observe that channel averaged velocity in the device is progressively reduced by increasing h_i. One can design a similar device using tens of progressively expanding channels. At the same time, it is possible to regulate

the channel averaged velocity in each channel using the channel height ratio, since

$$\bar{u_i} h_i = \bar{u_o} h_o = \dot{q}, \tag{5.3}$$

In the following, we decided to obtain $\bar{u_i} = (1.0 - 0.1 \times i) \times \bar{u_0}$ in each channel, and hence, we utilized $h_o = (1.0 - 0.1 \times i) \times h_i$. For example, this reduces the channel averaged velocity to $0.5 \times \bar{u_o}$ in the 5^{th} (main) channel by using $h_5 = 2 \times h_o$.

In order to investigate the effects of two-dimensional viscous flow, we numerically solved the Navier-Stokes equations in the device using channel expansion geometry described by $h_o = (1.0 - 0.1 \times i) \times h_i$. The stream-wise and span-wise velocity contours for $Re = 0.01$ flow are shown in figure 19 for two separate configurations, utilizing $\Delta L = 10 h_o$ (left) and $\Delta L = 4 h_o$ (right). The bottom row of figure 19 shows the streamwise velocity (u) variation at the centerline of the device (see also figure 18). We observe that $\Delta L = 10 h_o$ case results in step-like reduction in the centerline velocity, where u remains fairly constant between the channel expansion regions. This basically results in fully developed Poiseuille flow in between the channel expansion regions. On the other hand, the $\Delta L = 4 h_o$ geometry results in velocity contours similar to gradual expansion in a diffuser. This case results in (almost) linear decrease in the centerline velocity u with increased streamwise distance x. These two cases demonstrate two separate characteristics for the proposed device. The $\Delta L = 10 h_o$ and $\Delta L = 4 h_o$ cases lead to the "digitized" and "analog" versions of the device, respectively.

2. Electric Field and Electrokinetic Flow

The design includes electrodes located on the right and left sides of the device, where we apply an axial electric field in the channel. Ignoring the channel thickness effects, the device experiences *uniform* electric field. Under these conditions, the electroki-

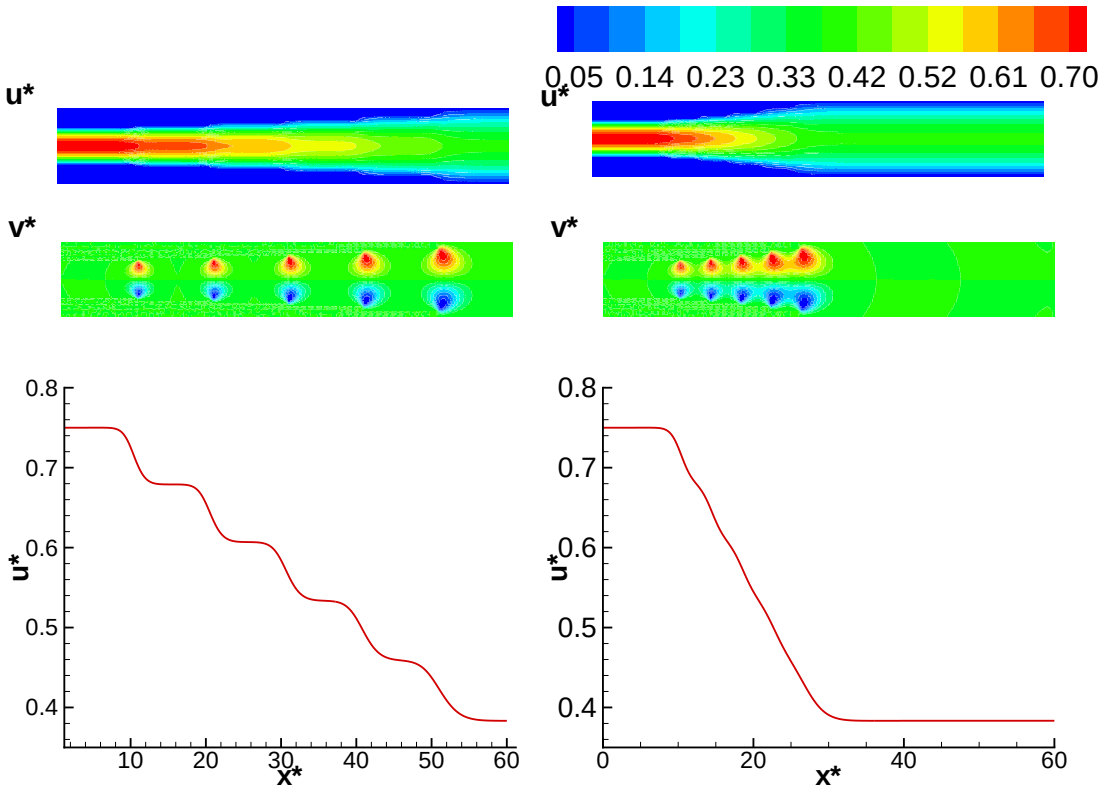

Fig. 19. Pressure driven flow velocity contours (u^*- stream wise; v^*- span wise) and the velocity distribution at channel centerline for $\Delta L = 10h_o$ (left column) case and $\Delta L = 4h_o$ (right column) case.

netic transport can be simply modeled using electrokinetic mobility μ_{ek} concept. For a given *uniform* electric field E, each specie i will experience a different electrokinetic velocity $u_{ek,i}$

$$u_{ek,i} = \mu_{ek,i}\vec{E}, \tag{5.4}$$

Due to the uniform axial electric field, the electrokinetic velocity of each specie is in the axial direction, and $u_{ek,i}$ is constant in the entire device. Electrokinetic mobility of charged species can be written as superposition of the species electrophoretic mobility μ_{ep}, and the electroosmotic mobility μ_{eo} of the buffer solution:

$$\mu_{ek} = \mu_{ep} + \mu_{eo}, \tag{5.5}$$

The electroosmotic flow (EOF) is generated when an axial electric field is imposed in presence of an ionized fluid that is in contact with a dielectric surface. Therefore, the electrically neutral buffer will experience electroosmotic motion. Depending on the zeta potential, the EOF will be towards the oppositely charged electrode. The EOF may seem to complicate the device operation. However, we plan to utilize an electrically neutral species as the EOF marker, similar to the capillary electrophoresis measurements. If we can simultaneously measure the electrokinetic mobilities of charged and electrically neutral species, we can directly calculate the electrophoretic mobilities of charged species using equation (5.5).

B. Electrokinetic/Hydrodynamic Focusing Process

The main idea of our device is to *counter-balance* the electrokinetic and pressure-driven flows to form a focusing point for each species. We demonstrate the electrokinetic/hydrodynamic focusing considering the case shown in figure 18. The electric

field is from left to right, and we will first ignore the possible adverse effects of the EOF for simplicity of our discussion (we will address EOF and experimental procedure separately). Under these circumstances, negatively charged particles are supplied from a reservoir downstream of the main channel, and they migrate upstream towards the anode. Although the electrokinetic velocity of each species is a constant in the entire device, species swimming upstream experience increased PDF in the opposite direction to their motion. This results in reduction of the species net velocity

$$u_{net} = u_{ep,i} + \bar{u_i}, \tag{5.6}$$

Since PDF is stronger in the upstream of the device, under the appropriate flowrate $\dot{q}$ and electric field E, we obtain a *focusing point*, where the species net velocity becomes zero. Using equations (5.2), (5.4), and (5.6) this leads to

$$\mu_{ek,i} = \frac{\dot{q}/E}{h_i}, \tag{5.7}$$

Since q and E are fixed, the maximum and minimum electrokinetic mobilities will be observed at the inner and outer channels, respectively. Specifically, using equation (5.7) we obtain

$$\frac{\mu_{ek,i}}{\mu_{ek,o}} = \frac{h_o}{h_i}, \tag{5.8}$$

This shows that we can control the device resolution simply by changing the number and position of the splitter channels (h_i). For example choosing $h_o = (1.0 - 0.1 \times i) \times h_i$, we imposed 10% mobility demarcations in each channel. In addition, using 5 channels we obtain a measurement range of $\frac{1}{2}\mu_{ek,o} \leq \mu_{ek} \leq \mu_{ek,o}$. Independent control over the flow rate and the applied electric field enables a wide range of possibilities for the maximum mobility value $\mu_{ek,o}$, as shown by equation (5.7). In addition, the mobility-range and precision is determined by the device geometry.

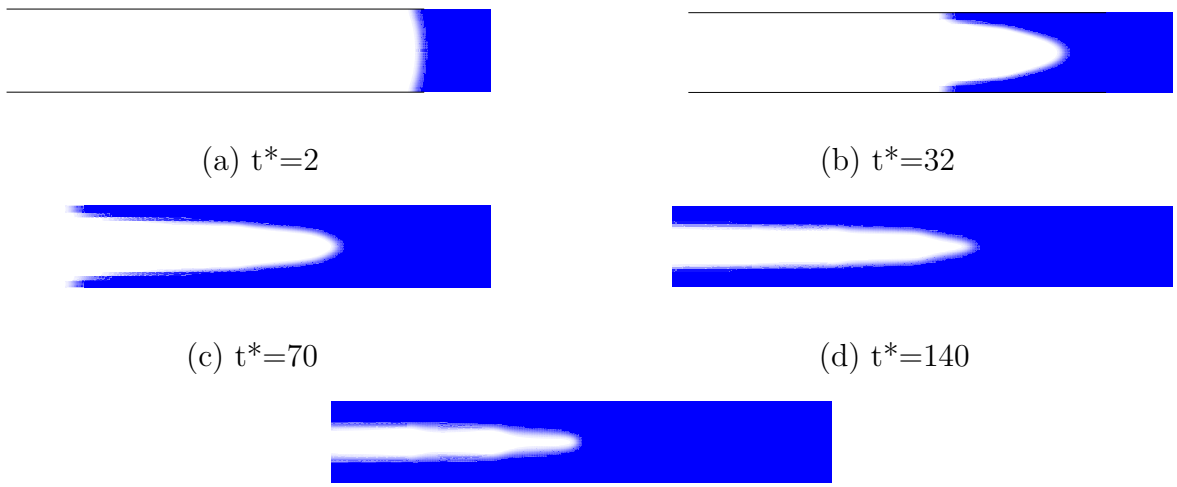

(a) t*=2

(b) t*=32

(c) t*=70

(d) t*=140

(e) t*=280

Fig. 20. The contour plots of charged species migration at various times, obtained for the "digitized" version of the device. Eventually, migration of the charged species stop at focusing point.

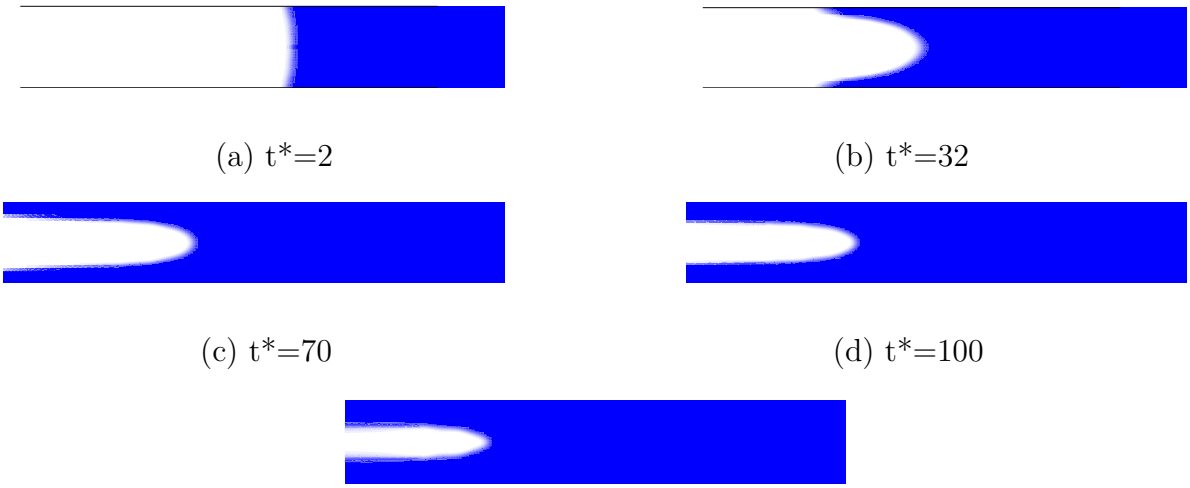

(a) t*=2 (b) t*=32

(c) t*=70 (d) t*=100

(e) t*=268

Fig. 21. The contour plots of charged species migration at various times, obtained for the "analog" version of the device. Eventually, migration of the charged species stop at focusing point.

Figures 20 and 21 show the snapshots of species migration at different times. $\Delta L = 10h_o$ and $\Delta L = 4h_o$ cases, respectively. Time t is normalized using the convective time scale based on the Helmholtz-Smoluchowski velocity (h_o/u_{HS}). The results at $t^* \geq 280$ correspond to long time behavior of the convective diffusive transport, and the focusing point (where the blue and white contours meet along the channel center line) is a stationary point, independent of time.

In figure 22 we present the electrokinetic/ hydrodynamic focusing obtained in two device configurations. The case with $\Delta L = 10h_o$ is shown on the left column, while the $\Delta L = 4h_o$ case is shown on the right. The contour plots are obtained for three different electrically charged species with electrokinetic mobilities of $\mu_A = 0.7\mu_0$, $\mu_B = 0.75\mu_0$, and $\mu_C = 0.8\mu_0$ at distinct focusing points in both devices. In here μ_0 is the mobility corresponding to the value of the maximum electrokinetic mobility

that would focus at the inner channel.

Using equation (5.6), we calculated the net species velocity at the centerline of each device. The bottom plots show variation of u_{net} as a function of the streamwise location x. Despite the small changes in the mobility, we observe three different focusing locations. The device with $\Delta L = 10h_o$ gives distinct focusing zones separated from each other. Hence, one can calculate the species mobility within a certain range $\Delta\mu_{ek}$ bounded by the theoretical mobility values of the neighboring channels. We identified this as the "digitized" version of the device. However, the second configuration ($\Delta L = 4h_o$) results in linear variation in species net velocity at the channel center. This enables continuous mobility information, and we identified this as the "analog" version of the device.

1. Experimental Procedure and Detection

The direction and magnitude of the electric field and PDF flowrate should be chosen as a function of the species charge polarity (positive or negative), which is not known apriory. Therefore, experiments can be started by applying an electric field in a preferred direction, and observing whether the mixture enters the micro-device or not. If the mixture (with unknown electrokinetic mobilities) does not enter the device, this may be due to the following two reasons: First, the electroosmotic flow may be stronger, and in the opposite direction to the electrophoretic transport. Second, the species may be oppositely charged than what was previously anticipated. These situations can be compensated either by reversing the electric field direction and/or by creating a pressure driven flow. For a mixture of positively and negatively charged multiple species, the device will *separate* the species based on their electrokinetic mobilities. For given PDF and electric field conditions, only the species with either the positive or negative mobilities will be able to enter the device. In fact, this may be

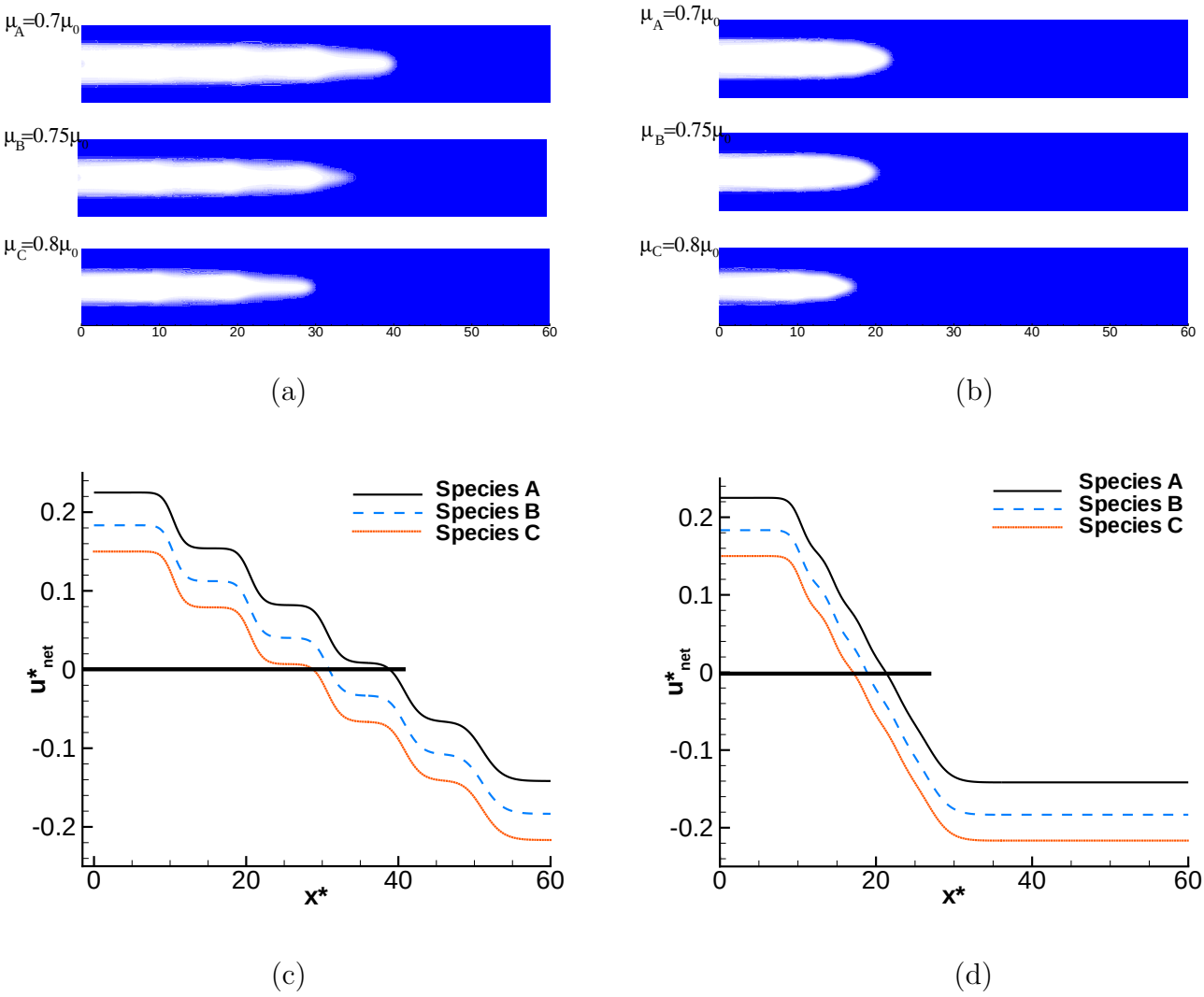

Fig. 22. Focusing point for (a) "digitized" version of the device and (b)"analog" version of the device. In both cases, three species with $\mu_A = 0.7\mu_0$, $\mu_A = 0.75\mu_0$, and $\mu_A = 0.8\mu_0$ were tested, where μ_0 is the mobility corresponding to the value that would focus at the inner channel. We also plot the corresponding centerline velocity for (c) the "digitized" and (d)"analog" versions of the device.

very useful for initial screening of the mixture. Adjusting the magnitude of the electric field and the flow-rate alter the sensitivity and range of the mobility measurements, as demonstrated in the next section.

2. Peclet Number Effect

The Reynolds number based on the PDF flow rate and the half channel height of main channel (h_5) is $Re = 0.005$. Despite this low Re, we imposed Peclet number $Pe = 1,000$, which corresponds to $Sc = 2 \times 10^5$. Such large Schmidt numbers are typical of large particles suspended in aqueous solutions, utilized in flow-tracing dyes, and bio-molecules. To investigate the Peclet number dependence of our device, we simulated two different cases at $Pe = 400$ and $Pe = 600$. In figure 23 we plot the concentration variation at the channel center as a function of the streamwise position x for both simulations. We observe that diffusion effects at the focusing point are insubstantial for $Pe \geq 400$. Therefore we expect very little effect of the species diffusion to our final results.

3. Multiple Charged Species Detection

One of the main attraction of our device is formation of stationary focusing points after the species migration process reaches to a steady-state. This enables superposition of results obtained separately so that we can measure multiple species mobility for dilute mixtures. Measurement of species concentration along the channel center line using fluorescent confocal microscopy will yield this information. Knowing the species concentration behavior along the channel center line enables us to determine the number of species and their relative concentration in the mixture. For example, given the concentration variation on the top left plot of figure 24, we observe that the given mixture has two components with distinct electrokinetic mobilities because we

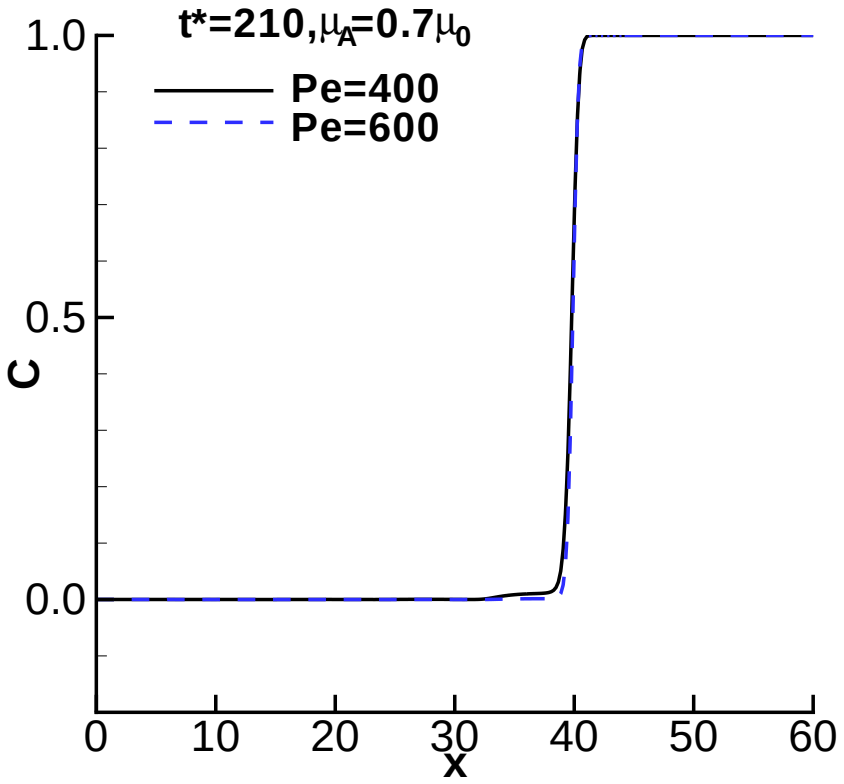

Fig. 23. Comparison for concentration distribution along the centerline of the micro-channel for $Pe = 400$ and $Pe = 600$.

observe two steps like variations. One component has relative concentration of 10% and it is focused at $x = 30$. From the focusing point we realize this component has mobility value of $\mu = 0.8\mu_0$ and μ_0 is the mobility of the inner channel. Likewise, the other component focusing at $x = 40$ is 90% of the mixture. This component has mobility value of $\mu = 0.7\mu_0$. In order to investigate the device resolution we present concentration variation at different relative concentration combinations. From the results of 90% vs 10%, 95% vs 5%, 99% vs 1%, and 55% vs 45% relative concentration compositions, we realize that our method can identify the composition with as small as 1 % resolution in the "digitized" (figure 24) and "analog" (figure 25) versions of our device.

C. Discussions

We demonstrated a new microfluidic device concept for electrophoretic mobility and (relative) concentration measurements of dilute mixtures. The device enables *stationary focusing points* for each species, where the locally applied pressure driven flow (PDF) counter balances the species' electrokinetic velocity. The location of the focusing point, along with the PDF flowrate and applied electric field reveals the electrokinetic mobility of each species. Simultaneous measurements of the electroosmotic mobility of an electrically neutral specie can be utilized to calculate the electrophoretic mobility of charged species. The proposed device utilizes constant sample feeding, and results in steady measurements. Hence, the results are independent of the initial sample distribution and the flow dynamics. In addition, the results are insensitive to the species diffusion for large Peclet number flows ($Pe > 400$). This enables measurement of the relative concentration levels of multiple species in dilute mixtures. Despite these advantages, the PDF results in strong species dispersion near channel

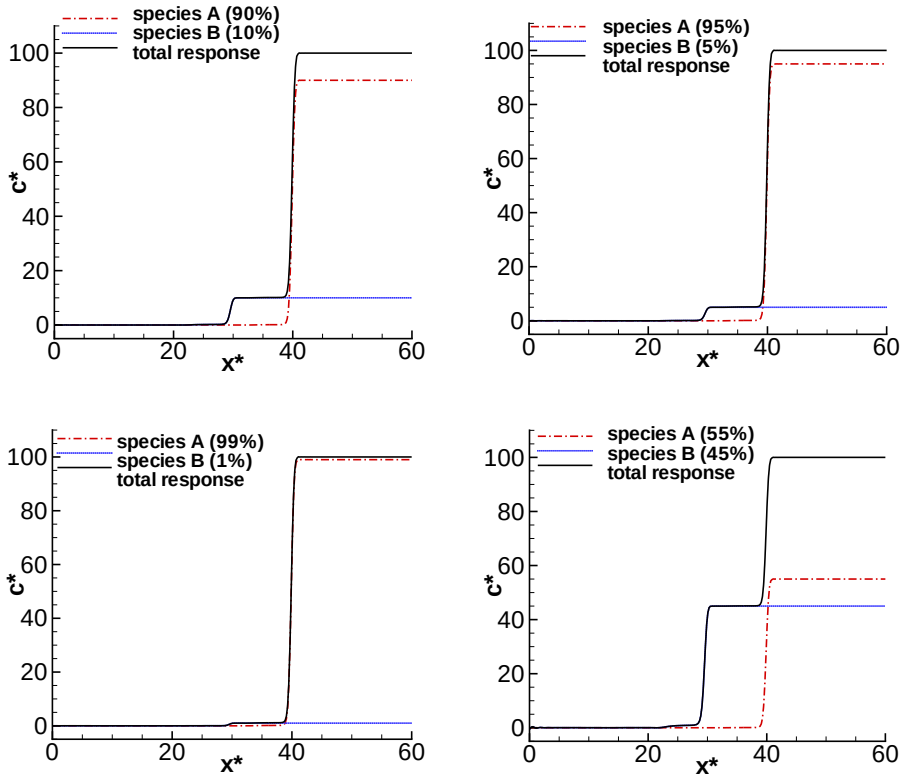

Fig. 24. Multiple species detection along the centerline of the micro-channel using superposition in "digitized" version of our device.

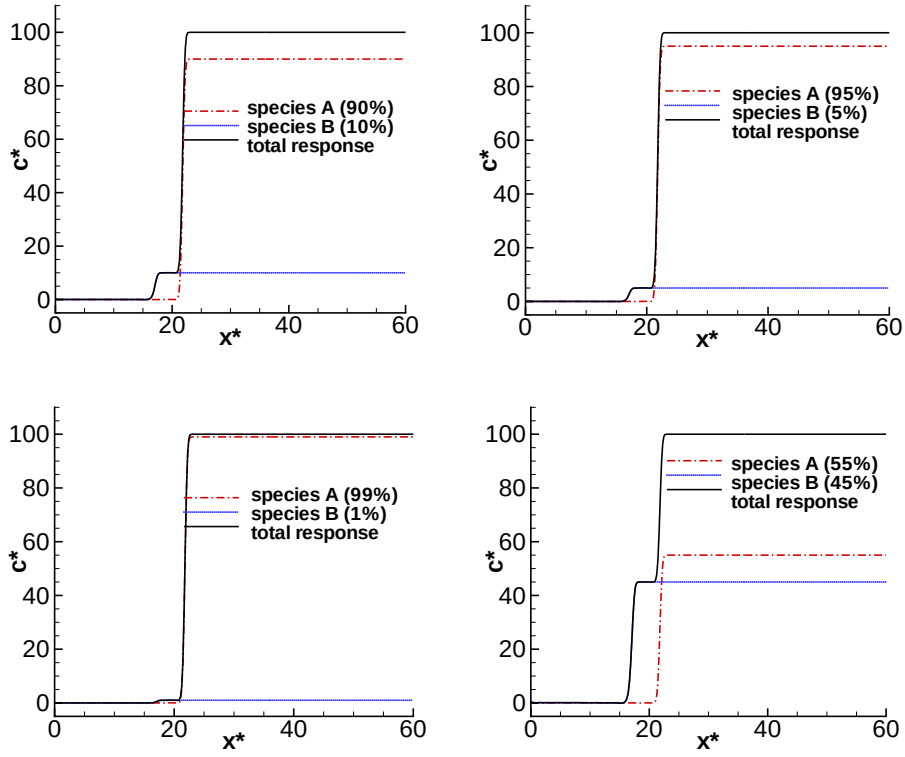

Fig. 25. Multiple species detection along the centerline of the micro-channel using superposition in "analog" version of the device.

surfaces. This problem can be resolved by utilization of large aspect ratio (width to height ratio) flow conduits, and fluorescence measurements using confocal microscopy sufficiently away from the device top surface. Based on these facts our device can identify multiple species in the mixture using the electrokinetic/hydrodynamic focusing.

CHAPTER VI

CONCLUSIONS

A. Summary and Discussion

We developed spectral element based numerical solvers to simulate electroosmosis and electrophoretic transport, and utilized this algorithm to simulate various micro-fluidic processes. Particularly we present two specific applications. One on flow and species transport control in grooved micro-channel and the other on hydrodynamic/electrokinetic focusing in a micro-fluidic device.

We demonstrated flow control concepts in a grooved micro-channel using selectively patterned, electroosmotically active surfaces and locally applied electric fields. This framework enables formation of rather complex flow patterns in simple micro-geometries. Ability to vary the electric field magnitude and its polarity also manifests time-dependent flow alterations, which results in flow and species transport control abilities. The results obtained in a single micro-groove constitute the proof of concept for flow and species transport control in an integrated serial micro-fluidic process, where *multiple species* can be trapped and released in *prescribed* amounts in a micro-channel with multiple grooves. The groove size determines volume of the entrapped species. In addition, each groove can simultaneously contain one or two species at the same time. The proposed flow and species transport control scheme allows control over the inter-species diffusion and mixing time and length scales by simply adjusting the electric field direction and its magnitude. We envision utilization of flow and species transport in a grooved micro channel, where combinatorial chemistry experiments can be performed using multiple grooves, where each groove can be addressed (filled, emptied or mixed) independently.

We also demonstrated a new microfluidic device concept for electrophoretic mobility and (relative) concentration measurements of dilute mixtures. The device enables *stationary focusing points* for each species, where the locally applied pressure driven flow (PDF) counter balances the species' electrokinetic velocity. The location of the focusing point, along with the PDF flowrate and applied electric field reveals the electrokinetic mobility of each species. Simultaneous measurements of the electroosmotic mobility of an electrically neutral specie can be utilized to calculate the electrophoretic mobility of charged species. The proposed device utilizes constant sample feeding, and results in steady measurements. Hence, the results are independent of the initial sample distribution and the flow dynamics. In addition, the results are insensitive to the species diffusion for large Peclet number flows ($Pe > 400$). This enables measurement of the relative concentration levels of multiple species in dilute mixtures. Despite these advantages, the PDF results in strong species dispersion near channel surfaces. This problem can be resolved by utilization of large aspect ratio (width to height ratio) flow conduits, and fluorescence measurements using confocal microscopy sufficiently away from the device top surface. Based on these facts and limitations our device can identify multiple species in a dilute mixture using electrokinetic/hydrodynamic focusing.

B. Suggestions for Future Work

Based on the present study, we suggest future work as follows:

- For numerical simulation, current study utilizes two dimensional model for numerical simulation. Three dimensional simulation is needed for realistic comparisons with experiments.

- Utilizing current numerical model, we can handle unsteady external electric

field. Based on this, we need to develop new ideas and devices to induce temporal flow modifications to create chaotic mixing with alternating current electroosmotic flow (ACEOF).

- In the future, actual devices of this study is needed to be fabricated and tested. Fabrication of large aspect ratio ($W >> h$) grooved channels with selective electrode and zeta potential patterned surfaces may require several processes that include micro-scale CNC machining, followed by the assembly of several interconnecting parts, and packaging.

- *Practical limitations*, such as the electrolysis of water, Joules heating, electrode oxidation, and possible pH fluctuations in the system should be studied and identified before fabrication and testing of the micro-fluidic devices presented in this thesis.

- For the flow and species control device, extension of the proposed method for electrically charged species requires considerations of the electrophoretic mobility of each species, where the combined hydrodynamic/electroosmotic velocity should overwhelm the local electrophoretic velocity. Therefore, design of a practical device to capture and release charged species would require a priory knowledge of the electrophoretic mobility of these species. Demonstration of charged species control in complex geometries will be needed in future studies.

REFERENCES

[1] R. F. Probstein, *Physiochemical Hydrodynamics: An Introduction*, New York: Wiley and Sons, 2nd edition, 1994.

[2] F. F. Reuss., "Sur un nouvel effet de l'electricite galvanique," *Memoires de la Societe Imperiale de Naturalistes de Moscou*, vol. 2, pp. 327–337, 1809.

[3] D. Burgreen and F. R. Nakache., "Eletrokinetic flow in ultrafine capillary silts," *J. Phys. Chem.*, vol. 68(5), pp. 1084–1091, 1964.

[4] H. Ohshima and T. Kondo, "Electrokinetic flow between two parallel plates with surface charge layers: Electroosmosis and streaming potential," *J. Colloids and Interface Science*, vol. 135(2), pp. 443–448, 1990.

[5] P. Dutta and A. Beskok, "Analytical solution of combined electroosmotic/ pressure driven flows in two-dimensional straight channels: Finite debye layer effects," *Analytical Chemistry*, vol. 73, pp. 1979–1986, 2001.

[6] C. L. Rice and R. Whitehead, "Electro kinetic flow in a narrow cylindrical capillary," *J. Phys. Chem.*, vol. 69(11), pp. 4017–4023, 1965.

[7] W. Y. Lo and K. Chan, "*Poisson-Boltzmann* calculations of ions in charged capillaris," *J. of Chem. Phys.*, vol. 69(11), pp. 4017–4023, 1965.

[8] H. J. Keh and Y. C. Liu, "Electrokinetic flow in a circular capillary with a surface charge layer," *J. Colloids and Interface Surfaces*, vol. 172, pp. 222–229, 1995.

[9] J. T. G. Overbeek, *Colloid Science*, Amsterdam: Elsevier Publishing Company, 1952.

[10] E. B. Cummings, S. K. Griffiths, R. H. Nilson, and P. H. Paul, "Conditions for similitude between the fluid velocity and electric field in electroosmotic flow," *Analytical Chemistry*, vol. 72(11), pp. 2526–2532, 2000.

[11] J. G. Santiago, "Electroosmotic flows in microchannels with finite inertial and pressure forces," *Analytical Chemistry*, vol. 73(10), pp. 2353–2365, 2001.

[12] P. Dutta and A. Beskok, "Analytical solution of time periodic electroosmotic flows: Analogies to Stokes' second problem," *Analytical Chemistry*, vol. 73, pp. 5097–5120, 2001.

[13] E. V. Dose and G. Guiochon, "Time scales of transient processes in capillary electrophoresis," *Journal of Chromatography*, vol. 652, pp. 263–275, 1993.

[14] O. Soderman and B. Jonsson, "Electroosmosis: velocity profiles in different geometries with both temporal and spatial resolution," *J. of Chem. Phys.*, vol. 105(23), pp. 10300–10311, 1996.

[15] N. G. Green, A. Ramos, A. Gonzalez, H. Morgan, and A. Castellanos., "Fluid flow induced by nonuniform AC electric fields in electrolytes on microelectrodes: I. experimental measurements," *Physical Review E*, vol. 61(4), pp. 4011–4018, 2000.

[16] A. Gonzalez, A. Ramos, N. G. Green, and A. Castellanos, "Fluid flow induced by nonuniform ac electric fields in electrolytes on microelectrodes: II. a linear double layer analysis," *Physical Review E*, vol. 61(4), pp. 4019–4028, 2000.

[17] V. M. Barrgan and C. R. Bauza, "Electroosmosis through a cation-exchange membrane: Effect of an AC perturbation on the electroosmotic flow," *J. of Colloid and Interface Science*, vol. 230, pp. 359–366, 2000.

[18] J. I. Molho, A. E. Herr, M. Desphande, J. R. Gilbert, M. G. Garguilo, P. H. Paul, P. M. John, T. M. Woudenberg, and C. Connel, "Fluid transport mechanisms in micro fluidic devices," in *ASME International Mechanical Engineering Congress and Exposition*, ASME, pp. 69–75, 1998.

[19] P. H. Paul, M. G. Graguilo, and D. J. Rakestraw, "Imaging of pressure and electrokinetically driven flows through open capillaries," *Analytical Chemistry*, vol. 70(13), pp. 2459–2467, 1998.

[20] E. B. Cummings, S. K. Griffiths, and R. H. Nilson., "Irrotationality of uniform electroosmosis,"*in Proc. SPIE Microfluidic Devices and Systems II* , SPIE, Santa Clara, CA, pp. 180–189, 1999.

[21] M. J. Kim, K. D. Kihm, and A. Beskok, "A comparative study of μ-PIV measurements and numerical simulations of electroosmotic flows in various micro-channel configurations," *Experiments in Fluids*, vol. 33, pp. 170–180, 2002.

[22] A. Singh, E. B. Cummings, and D. J. Throckmorton, "Flourescent liposome flow markers for microscale particle-image velocimetry," *Analytical Chemistry*, vol. 73(5), pp. 1057–1061, 2001.

[23] A. E. Herr, J. I. Molho, J. G. Santiago, M. G. Mungal, T. W. Kenny, and M. G. Garguilo, "Electroosmotic capillary flow with non uniform zeta potential," *Analytical Chemistry*, vol. 72(5), pp. 1053–1057, 2000.

[24] C. Yang and D. Li, "Analysis of electrokinetic effects on the liquid flow in rectangular microchannels," *J. of Colloid and Interface Science*, vol. 143, pp. 339–353, 1998.

[25] N. A. Patankar and H. H. Hu, "Numerical simulation of electroosmotic flow," *Analytical Chemistry*, vol. 70(9), pp. 1870–1881, 1998.

[26] F. Bianchi, R. Ferrigno, and H. H. Girault, "Finite element simulation of an electroosmotic-driven flow division at a t-junction of microscale dimension," *Analytical Chemistry*, vol. 72(9), pp. 1987–1993, 2000.

[27] P. Dutta, A. Beskok, and T. C. Warburton, "Numerical simulation of mixed electroosmotic/pressure driven microflows," *Numerical Heat Transfer, Part-A: Applications*, vol. 41(2), pp. 131–148, 2002.

[28] P. Dutta, A. Beskok, and T. C. Warburton, "Electroosmotic flow control in complex microgeometries," *J. Microelectromechanical Systems*, vol. 11(1), pp. 36–44, 2002.

[29] J. Horvath and V. Dolnik, "Polymer wall coatings for capillary electrophoresis," *Electrophoresis*, vol. 22, pp. 644–655, 2001.

[30] P. G. Righetti, C. Gelfi, B. Verzola, and L. Castelletti, "The state of art of dynamic coatings," *Electrophoresis*, vol. 22, pp. 603–611, 2001.

[31] Y. Liu, J. C. Fanguy, J. M. Bledsoe, and C. S. Henry, "Dynamic coating using polyelectrolyte multilayers for chemical control of electroosmotic flow in capillary electrophoresis microchips," *Analytical Chemistry*, vol. 72(24), pp. 5939–5944, 2000.

[32] D. Kaniansky, M. Masar, and J. Bielcikova, "Electroosmotic flow separation for capillary zone electrophoresis in a hydrodynamically closed separation system," *Journal of Chromatography A*, vol. 792, pp. 483–494, 1997.

[33] M. A. McClain, C. T. Culbertson, S. C. Jacobson, and J. M. Ramsey, "Flow cytometry of escherichia coli on microfluidic devices," *Analytical Chemistry*, vol. 73(21), pp. 5334–5338, 2001.

[34] S. L. R. Barker, D. Ross, M. J. Tarlov, M. Gaitan, and L. E. Locasio, "Control of flow direction in microfluidic devices with polyelectrolyte multilayers," *Analytical Chemistry*, vol. 72(24), pp. 5925–5929, 2000.

[35] R. B. M. Schasfoort, S. Schlautmann, J. Hendrikse, and A. V. D. Berg, "Electroosmotic flow in a microcapillary with one solution displacing another solution," *J. of Colloid and Interface Science*, vol. 242, pp. 264–271, 2001.

[36] J. S. Buch, P. C. Wang, D. L. DeVoe, and S. L. Lee, "Field-effect flow control in a polydimethylsiloxane-based microfluidic system," *Electrophoresis*, vol. 22, pp. 3902–3907, 2001.

[37] S. C. Jacobson, T. E. McKnight, and J. M. Ramsey, "Microfluidic devices for electrokinetically driven parallel and serial mixing," *Analytical Chemistry*, vol. 71, pp. 4455–4459, 1999.

[38] C. Yang, C. B. Ng, and V. Chan, "Transient analysis of electroosmotic flow in a slit microchannel," *J. of Colloid and Interface Science*, vol. 248(2), pp. 524–527, 2002.

[39] S. Qian and H. H. Bau, "A chaotic electroosmotic stirrer," *Analytical Chemistry*, vol. 74, pp. 3616–3625, 2002.

[40] H. Aref, "Stirring by chaotic advection," *J. Fluid Mech.*, vol. 143, pp. 1–21, 1984.

[41] H. Aref and S. Balachandar, "Chaotic advection in a Stokes flow," *Phys. Fluid*, vol. 29, pp. 3515–3521, 1986.

[42] W. L. Tseng and H. T. Chang, "A new stategy for optimizing sensitivity, speed, and resolution in capillary electrophoretic separation of DNA," *Electrophoresis*, vol. 22, pp. 763–770, 2001.

[43] K. Kleparnik, Z. Mala, and P. Bocek, "Fast separation of DNA sequencing fragments in highly alkaline solutions of linear polyacrylamide using electrophoresis in bare silica capillaries," *Electrophoresis*, vol. 22, pp. 783–788, 2001.

[44] M. J. Cunningham, "Genomics and proteomics- The new millennium of drug discovery and development," *J. Pharmacol. Toxicol. Methods*, vol. 44(1), pp. 291–300, 2000.

[45] M. Melvin, *Electrophoresis*, London: John Wiley and Sons Inc, 1987.

[46] P. G. Righetti, *Isoelectric Focussing: Theory, Methodology and Applications*, Amsterdam: Elsevier Biomedical, 1983.

[47] K. Macounova, C. R. Cabrera, M. R. Holl, and P. Yager, "Generation of natural pH gradients in microfluidic channels for use in isoelectric focusing," *Analytical Chemistry*, vol. 72(16), pp. 3745–3751, 2000.

[48] K. Macounova, C. R. Cabrera, and P. Yager, "Concentration and separation of proteins in microfluidic channels on the basis of transverse IEF," *Analytical Chemistry*, vol. 73(7), pp. 1627–1633, 2001.

[49] C. R. Cabrera, B. Finlayson, and P. Yager, "Formation of natural pH gradients in a microfluidic device under flow conditions: Model and experimental validation," *Analytical Chemistry*, vol. 73(3), pp. 658–666, 2001.

[50] R. Westermeier, *Electrophoresis in Practice*, New York: VCH Publishers Inc, 1990.

[51] P. Janos, "Role of chemical equilibria in the capillary electrophoresis of inorganic substances," *Journal of Chromatography A*, vol. 834, pp. 3–20, 1999.

[52] N. A. Polson and M. A. Hayes, "Electroosmotic flow control of fluids on a capillary electrophoresis microdevice using an applied external voltage," *Analytical Chemistry*, vol. 72(5), pp. 1088–1092, 2000.

[53] R. J. Hunter, *Zeta Potential in Colloid Science: Principles and Applications*, New York: Academic Press Inc, 1981.

[54] S. C. Jacobson, J. P. Alarie, and J. M. Ramsey, "Electrokinetic transport through nanometer deep channels," *Micro Total Analysis Systems*, pp. 57–59, 2001.

[55] J. A. Strantton, *Electromagnetic Theory*, New York: McGraw Hill, 1941.

[56] S. V. Ermakov, S. C. Jacobson, and J. M. Ramsey, "Computer simulation of electrokinetic transport in micro fabricated channel structures," *Analytical Chemistry*, vol. 70(21), pp. 4494–4504, 1998.

[57] S. V. Ermakov, S. C. Jacobson, and J. M. Ramsey, "Computer simulation of electrokinetic mass transport in microfabricated fluidic devices," *in Proc. of Modeling and Simulation of Microsystems*, Puerto Rico, pp. 534–537, 1999.

[58] M. Jansson, A. Emmer, and J. Roeraade, "Some design considerations in miniaturized electrokinetic separation systems," *J. High Resolut. Chromatogr.*, vol. 12(12), pp. 797–807, 1989.

[59] O. A. Palusinski, A. Graham, R. A. Mosher, M. Bier, and D. A. Saville, "Theory of electrophoretic separations, part II: Construction of a numerical simulation scheme and it's applications," *AICHE Journal*, vol. 32(2), pp. 215–223, 1986.

[60] S. V. Ermakov, O. S. Mazhorova, and Y. P. Popov, "Mathematical modeling of the electrophoretic separation of biological mixtures," *Translated from Differentsial'nye Uravneniya*, vol. 12, pp. 2129–2137, 1992.

[61] T. M. Grateful and E. N. Lightfoot, "Finite difference modelling of continuous-flow electrophoresis," *Journal of Chromatography*, vol. 594, pp. 341–349, 1992.

[62] S. V. Ermakov, M. S. Bello, and P. G. Righetti, "Numerical algorithms for capillary electrophoresis," *Journal of Chromatography A*, vol. 661, pp. 265–278, 1994.

[63] S. V. Ermakov, S. C. Jacobson, and J. M. Ramsey, "Computer simulations of electrokinetic injection techniques in microfluidic devices," *Analytical Chemistry*, vol. 72(15), pp. 3512–3517, 2000.

[64] M. G. Giridharan and A. Krishnan, "An implicit numerical model for electrophoretic systems," *Proc. ASME International Mechanical Engineering Congress and Exposition, Micro-Electro-Mechanical Systems (MEMS)*, ASME, pp. 61–68, 1998.

[65] S. Krishnamoorthy and M. G. Giridharan, "Analysis of sample injection and band-broadening in capillary electrophoresis microchips,"*2000 in Int'l. Conference on Modeling and Simulation of Microsystems (MSM)*, San Diego, CA , pp. 61–68,2000.

[66] A. Beskok, A. and T. C. Warburton, "Unstructured hp finite-element scheme for fluid flow and heat transfer in moving domains," *J. Computational Physics*, vol. 174, pp. 492–509, 2001.

[67] G. E. Karniadakis, M. Israeli, and S. A. Orszag, "High-order splitting methods for the incompressible Navier-Stokes equations," *J. Computational Physics*, vol. 97, pp. 414–443, 1991.

[68] G. E. Karniadakis and S. J. Sherwin, *Spectral/HP Element Methods for CFD*, Oxford: Oxford University Press, 1999.

[69] T. C. Warburton, "Spectral/hp methods on polymorphic multi-domains: Algorithms and applications," Ph.D. dissertation, Brown University, Providence, RI, 1999.

[70] L. W. Ho, "A legendre spectral element method for simulation of incompressible unsteady free-surface flows," Ph.D. dissertation, Massachusetts Institute of Technology, Cambridge, MA, 1989.

[71] R. Lohner and C. Yang, "Improved ALE mesh velocities for moving bodies," *Comm. Num. Meth. Eng. Phys.*, vol. 12, pp. 599–608, 1996.

[72] P. Dutta, "Numerical modeling of electroosmotically driven flows in complex micro-geometries," Ph.D. dissertation, Texas A&M University, College Station, TX, 2001.

[73] G. E. Karniadakis, A. Beskok, and N. Aluru, *Microflows and Nanoflows: Fundamentals and Simulation*, New York: Springer-Verlag, 2005.

[74] R. B. Schasfoort, S. Schlautmann, J. Hendrikse, and A. van den Berg, "Field-effect flow control for microfabricated fluidic networks," *Science*, vol. 5441, pp. 942–945, 1999.

[75] S. Taneda, "Visualization of the separating Stokes flows," *J. Phys. Soc. Japan*, vol. 46, pp. 1935–1942, 1979.

[76] X. Niu, and Y. K. Lee, "Efficient spatial-temporal chaotic mixing in microchannels," *J. Micromech. Microeng.*, vol. 13, pp. 454–462, 2003.

VITA

Jungyoon Hahm was born in Kangneung City, Korea in 1974. He graduated with a B.S. degree in Mechanical Engineering from Hong-Ik University, Seoul, Korea in 1997 and he got his M.S. from the same department in 1999. He was an assistant researcher in the Tribology Research Center. He got another M.S. from the Mechanical Engineering department of the University of Wisconsin-Madison, where he worked at the Engine Research Center. In August 2001, he joined the Department of Mechanical Engineering at Texas A&M University. He was a research assistant in the bio-micro-fluidics laboratory. He graduated with a Ph.D. degree in Mechanical Engineering, in August 2005. Jungyoon Hahm can be contacted through Dr. Ali Beskok at the Mechanical Engineering Department, Texas A&M University, College Station, 77843-3123.